Available online at www.sciencedirect.com
ScienceDirect
International Journal of Solids and Structures 44 (2007) 298–319
INTERNATIONAL JOURNAL OF SOLIDS and STRUCTURES
www.elsevier.com/locate/ijsolstr

# Design and analysis of a smart composite pipe joint system integrated with piezoelectric layers under bending

Jinquan Cheng [a,b,*], Xiaoxia Wu [b], Guoqiang Li [a], Su-Seng Pang [a], Farid Taheri [b]

[a] Department of Mechanical Engineering, Louisiana State University, Baton Rouge, LA 70803, United States
[b] Department of Civil Engineering, Dalhousie University, 1360 Barrington Street, Halifax, NS, Canada B3J 1Z1

Received 23 July 2005; received in revised form 6 April 2006
Available online 27 April 2006

**Abstract**

Incorporating with the high electro-mechanical coupling performance of piezoelectric materials, design and analysis of an adhesively bonded smart composite pipe joint system were conducted. In this joint system, piezoelectric layers were integrated into the joint coupler in order to reduce stress concentration in the joint adhesive layer. To theoretically verify the composite action and efficiency of the integrated piezoelectric layers, an electro-mechanical model based on the first-order shear deformation theory was established. This model was able to clarify the energetic characteristics of the proposed joint system on the improvement in the joint strength, which was under the action of a bending moment at the joint ends. The state-space method was utilized to obtain the final analytical solutions, including the peel and shear stress distributions in the adhesive layer. Finally, some numerical examples were calculated to evaluate the effect of the detailed stacking sequence and size of the integrated piezoelectric layers on reducing the stress concentration in the adhesive layer as well as the applied electric fields. These numerical results validated the integrity of the developed adhesively bonded smart composite pipe joint system.
© 2006 Elsevier Ltd. All rights reserved.

*Keywords:* Pipe joint; Composite; Adhesive; Smart materials and structures; Stress analysis; Piezoelectrics

## 1. Introduction

With the advancement of adhesive materials and techniques in adhesive bonding in the past decades, a number of adhesively bonded joint systems have been increasingly applied in engineering structures, such as the single-lap joint, single-strap joint, double lap joint and pipe joint in aeronautics, automotive, civil engineering structures etc. Recently, with the inflated energy consumption, the exploitation and transport of oil and gas have become one of the hottest topics in the world. As is well known, adhesively bonded pipeline networks, including adhesively bonded socket joint, butt-and-strap joint and flanged joint etc., have been successfully

* Corresponding author.
*E-mail address:* hitcjq@hotmail.com (J. Cheng).

0020-7683/$ - see front matter © 2006 Elsevier Ltd. All rights reserved.
doi:10.1016/j.ijsolstr.2006.04.021

applied as one of the most low-cost and efficient transport methods in the industry. Evidently, for any type of adhesively bonded joint systems, stress transfer is generally through the adhesive layer bond-line via peel and shear stresses. And, a significant peel/shear stress concentration always exists in the edge region at the adhesive layer bond-line, which has been theoretically and experimentally verified by previous works (Goland and Reissner, 1944; Hart-Smith, 1973; Adams and Wake, 1984; Tsai and Morton, 1994). Thereby, the stress concentration in the edge region at the adhesive layer is the lethiferous reason of inducing adhesively bonded joint failure. In order to prevent the joint from premature failure, reducing the stress concentration becomes crucial. Although many theoretical, numerical and experimental analyses have been conducted in the literatures on adhesively bonded beam and plate joint systems, only a limited number of experimental and theoretical studies have been conducted to investigate the adhesively bonded pipe joint system subjected to complicated external tension, bending and torsion loading, including Adams and Peppiatt (1977), Chen and Cheng (1992a), Chen and Cheng (1992b), Choi and Lee (1997), Lee and Oh (1999), Yang (2000), Yang et al. (2002), and Pugno and Carpinteri (2003) etc. Therefore, how to improve the strength capacity and reliability of such joint systems is still the most desired aim in engineering community. Some traditional and preventive enhancement methods, including rounding off the sharp edges, spewing fillets and tapering of the adherends etc. (Hart-Smith, 1983; Roberts, 1989; Cheng et al., 1991), have been successfully applied in engineering structures. Furthermore, some other mechanical stiffening methods have also been introduced to improve the joint strength. For instance, Albat and Romilly (1999) have used some reinforcing patches to reduce the stress concentration in adhesive layers. However, all of the above mentioned strength enhancement methods, namely, the traditional geometric improvement or mechanical stiffening methods are passive enhancement methods. They are unable to survive sudden and extreme loadings. Therefore, in the present paper, an adaptive adhesively bonded pipe joint system was designed and analyzed to create a smart and active enhancement and protection for such pipe joint system using high electro-mechanic coupling piezoelectric materials.

Smart materials have been successfully applied as sensors and actuators in the engineering structures, such as Crawley and de Luis (1987), Lee and Moon (1990), Cheng et al. (2000), Wu et al. (2001), Batra and Geng (2001), Luo and Tong (2002), Zhou and Wang (2002), Zhou et al. (2003), Cheng et al. (2005a,b) etc. However, few studies can be found in the open literatures on the application of smart materials in adhesive joint systems. Recently, Cheng and Taheri (2005, 2006) have utilized piezoelectric materials to successfully improve the adhesively bonded beam-like joint system in theory and experiment, and then introduced the adaptive strength improvement method for the conventional adhesively bonded joint system. From the authors' previous works, it is verified that the peel/shear stress concentration in the adhesive layer can be remarkably reduced through actively adjusting applied electric fields in the integrated piezoelectric patches/layers. Therefore, it is a reasonable development to integrate the piezoelectric materials into the connection coupler of a common pipe joint system. It is expected that this adhesively bonded smart pipe joint system will reduce the stress concentration and enhance the strength of the pipe joint.

In this paper, an idealized adhesively bonded smart composite pipe joint system, which had an adaptive connection coupler that was integrated with some piezoelectric layers as actuators, was firstly developed. In order to conveniently design and optimize the proposed smart joint structure, an analytical model based on the first-order shear deformation theory was set up to obtain fundamental expressions for the joint system. This model was able to consider the electro-mechanical coupling effect of the integrated piezoelectric layers. Further, when the joint was subjected to a bending moment at the joint end, a basic solution process was presented in detail. The state-space method was employed to obtain the analytical solutions, including the peel and shear stress distributions in the adhesive layer bond line. Finally, some detailed numerical simulations were conducted to demonstrate the design and optimization of the joint system under the combined end bending moment and electric fields, including the effect of the thickness and stacking sequence of the integrated piezoelectric layers.

## 2. Basic smart pipe joint structure and fundamental equations

### 2.1. Basic smart composite pipe joint structure

In general, an adhesively bonded pipe joint system is composed of a main pipe, connection coupler and adhesive layer, such as a single-strap type pipe joint, as shown in Fig. 1. In theory, such a pipe joint system

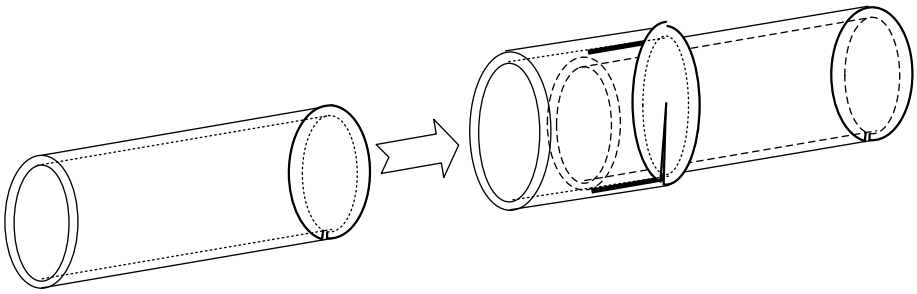

Fig. 1. A schematic view of a typical pipe joint system.

can be approximated as a symmetric or quasi-symmetric joint structure even though the material properties and geometries of the pipe and coupler are different from each other. As mentioned above, in order to reduce the stress concentration in the adhesive layer bond line, many traditional passive reinforcement methods have been developed to enhance the strength capacity of such joints. In this study, we proposed to develop an actively enhanced pipe joint – a smart composite pipe joint system, in which high electro-mechanical coupling piezoelectric materials are integrated as actuators to adaptively reduce the peel/shear stresses concentration in the adhesive layer. It is well known that the peel/shear stress concentrations in the adhesive layer can be intensively reduced by adjusting the applied forces and moments at the joint edges as well as the geometries and material properties of the adherent and adhesive (Roberts, 1989). Therefore, on the basis of our findings in previous studies (Cheng and Taheri, 2005, 2006), together with the high electro-mechanical coupling effect of the piezoelectric materials, a smart composite pipe joint system with a smart connection coupler integrated with piezoelectric reinforced layers can be constructed, as shown in Figs. 1 and 3(b), was proposed. Since the general piezoelectric ceramics are brittle, it is difficult to integrate them into the joint coupler (Cheng et al., in press). Thus considering the manufacture convenience of the pipe joint, we can use piezoelectric particle/fiber reinforced composite materials in the present application. For an example of an adhesively bonded socket joint, we can directly integrate the piezoelectric particle/fiber reinforced composite layer into the composite socket part as the actuator. In the present smart pipe joint system, adjusting externally applied electric fields in the integrated active piezoelectric layers can induce relevant deformation in the smart laminates to cause additional force and moment at the joint edges so as to reduce/increase the stress concentration in the adhesive layer. It is undoubted that the stacking sequence of the reinforced piezoelectric layers in the connection coupler should have a significant effect on the efficiency of the smart joint, so do the piezoelectric layer thickness and applied electric fields. In order to validate the composite action and efficiency of the integrated piezoelectric reinforced layers, an analytical model based on the first-order shear deformation theory will be established to carry out the peel and shear stress distribution analysis in the adhesive layer under the electro-mechanical loading in the following sections.

### 2.2. Fundamental equations

In order to verify the efficiency of the smart composite pipe joint system, the first-order shear deformation theory is employed to model the smart joint and further obtain the relevant fundamental equations. Based on the assumption of the first-order shear deformation theory for a moderately thick shell, the displacement fields can be assumed as functions of the mid-plane displacements $(u_0, v_0, w_0)$ in the following forms:

$$u(\varsigma, \xi, z) = u_0(\varsigma, \xi) + z\phi(\varsigma, \xi) \tag{1a}$$

$$v(\varsigma, \xi, z) = v_0(\varsigma, \xi) + z\varphi(\varsigma, \xi) \tag{1b}$$

$$w(\varsigma, \xi, z) = w_0(\varsigma, \xi) \tag{1c}$$

where $(u_0, v_0, w_0)$ are the displacements of a point $(\zeta, \xi, 0)$ on the mid-plane of the shell, and, $(\phi, \varphi)$ are the rotations of a normal to the reference surface as shown in Fig. 2.

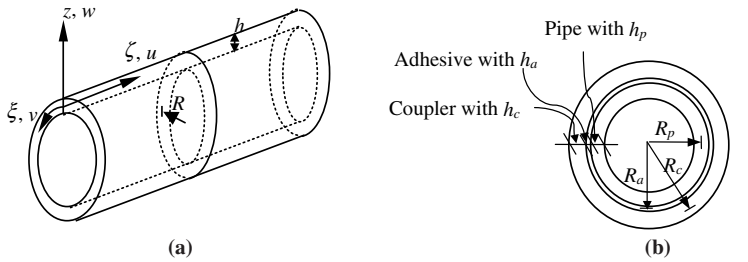


Fig. 2. A schematic geometric view of the pipe joint: (a) an isometric view and (b) a cross-sectional view.

In terms of the strain–displacement relationships in the general shell coordinate system as shown in Fig. 2, the strain can be expressed as follows:

$$\varepsilon_\varsigma = \varepsilon_1 = \frac{\partial u}{\partial \varsigma} = \frac{\partial u_0}{\partial \varsigma} + z\frac{\partial \phi}{\partial \varsigma}; \tag{2a}$$

$$\varepsilon_\xi = \varepsilon_2 = \frac{w}{R+z} + \frac{R}{R+z}\frac{\partial v}{\partial \xi} = \frac{w}{R+z} + \frac{R}{R+z}\left(\frac{\partial v_0}{\partial \xi} + z\frac{\partial \varphi}{\partial \xi}\right); \tag{2b}$$

$$\varepsilon_z = \varepsilon_3 = \frac{\partial w}{\partial z} = 0; \tag{2c}$$

$$\varepsilon_{\xi z} = \varepsilon_4 = \gamma_{23} = \frac{R}{R+z}\frac{\partial w}{\partial \xi} + \frac{\partial v}{\partial z} - \frac{v}{R+z} = \frac{R}{R+z}\frac{\partial w}{\partial \xi} - \frac{v_0}{R+z} + \frac{R}{R+z}\varphi; \tag{2d}$$

$$\varepsilon_{\varsigma z} = \varepsilon_5 = \gamma_{13} = \frac{\partial u}{\partial z} + \frac{\partial w}{\partial \varsigma} = \phi + \frac{\partial w_0}{\partial \varsigma}; \tag{2e}$$

$$\varepsilon_{\varsigma\xi} = \varepsilon_6 = \gamma_{12} = \frac{R}{R+z}\frac{\partial u}{\partial \xi} + \frac{\partial v}{\partial \varsigma} = \frac{R}{R+z}\frac{\partial u_0}{\partial \xi} + \frac{zR}{R+z}\frac{\partial \phi}{\partial \xi} + \frac{\partial v_0}{\partial \varsigma} + z\frac{\partial \varphi}{\partial \varsigma} \tag{2f}$$

where $R$ denotes the mid-plane radius for different parts of the joint, such as $R_p$ and $R_c$ are the radius of the mid-plane for the pipe wall and connection coupler wall, respectively; see Fig. 3.

Considering the effect of piezoelectric layers with the poling direction along the $z$-axis and fiber distribution angle of the $k$th layer in the composite laminated pipe, the common stress–strain relationships of the $k$th lamina can be obtained in the shell coordinate system as

$$\begin{Bmatrix} \sigma_1 \\ \sigma_2 \\ \sigma_4 \\ \sigma_5 \\ \sigma_6 \end{Bmatrix}^k = \begin{bmatrix} \overline{Q}_{11} & \overline{Q}_{12} & 0 & 0 & \overline{Q}_{16} \\ \overline{Q}_{12} & \overline{Q}_{22} & 0 & 0 & \overline{Q}_{26} \\ 0 & 0 & \overline{Q}_{44} & \overline{Q}_{45} & 0 \\ 0 & 0 & \overline{Q}_{54} & \overline{Q}_{55} & 0 \\ \overline{Q}_{16} & \overline{Q}_{16} & 0 & 0 & \overline{Q}_{66} \end{bmatrix}^k \begin{Bmatrix} \varepsilon_1 \\ \varepsilon_2 \\ \varepsilon_4 \\ \varepsilon_5 \\ \varepsilon_6 \end{Bmatrix} - \begin{Bmatrix} \bar{e}_{31} \\ \bar{e}_{32} \\ 0 \\ 0 \\ \bar{e}_{36} \end{Bmatrix}^k E_3^k \tag{3}$$

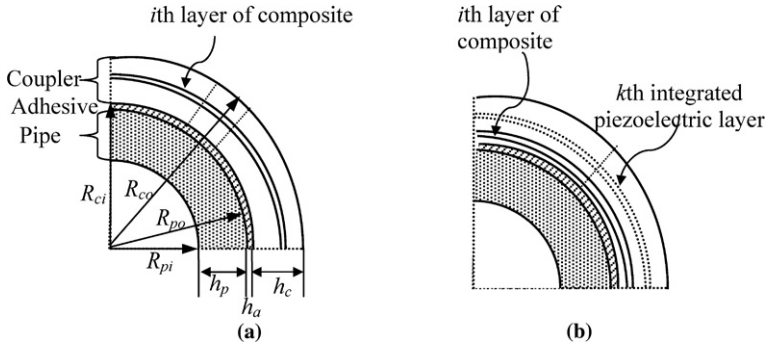


Fig. 3. The conventional pipe-joint system (a) and the proposed smart pipe joint system integrated with the piezoelectric layer (b).

where the superscript "$k$" denotes the $k$th layer of the laminate panel. $\overline{Q}_{ij}$ are the transformed stiffnesses and can be obtained from the stacked lamina. $E_3^k$ is the applied electric field in the $k$th actuating piezoelectric layer. It is noted that the piezoelectric coefficients are equal to zero in the elastic layer. Because most of the reinforcements used in engineering are orthotropic, including chopped-strand mats, woven roving, unidirectional fabrics etc., the stress–strain relationships of the pipe walls can be approximately described in the following forms:

$$\begin{Bmatrix} \sigma_1 \\ \sigma_2 \\ \sigma_6 \end{Bmatrix}^k = \begin{bmatrix} \overline{Q}_{11} & \overline{Q}_{12} & 0 \\ \overline{Q}_{12} & \overline{Q}_{22} & 0 \\ 0 & 0 & \overline{Q}_{66} \end{bmatrix}^k \begin{Bmatrix} \varepsilon_1 \\ \varepsilon_2 \\ \varepsilon_6 \end{Bmatrix} - \begin{Bmatrix} \bar{e}_{31} \\ \bar{e}_{32} \\ 0 \end{Bmatrix}^k E_3^k \tag{4a}$$

$$\begin{Bmatrix} \sigma_4 \\ \sigma_5 \end{Bmatrix}^k = \begin{bmatrix} K\overline{Q}_{44} & 0 \\ 0 & K\overline{Q}_{55} \end{bmatrix}^k \begin{Bmatrix} \varepsilon_4 \\ \varepsilon_5 \end{Bmatrix} \tag{4b}$$

For a general laminate, the forces and moments can be deduced from the stress resultant by integration of the stresses along the thickness. Considering the effect of the integrated piezoelectric layers on different parts of the smart composite pipe joint system, the forces and moments can be obtained as follows:

$$\begin{aligned} N_{i\varsigma} = N_{i11} &= \int_{-\frac{h_i}{2}}^{\frac{h_i}{2}} \frac{(R_i+z)}{R_i}\sigma_1 \,\mathrm{d}z = \sum_{k=1}^{n}\int_{z_k}^{z_{k+1}} \frac{(R_i+z)}{R_i}(\overline{Q}_{11}^k\varepsilon_1 + \overline{Q}_{12}^k\varepsilon_2 - \bar{e}_{31}^k E_3^k)\,\mathrm{d}z \\ &= A_{i11}\frac{\partial u_{i0}}{\partial\varsigma} + B_{i11}\frac{\partial\phi_i}{\partial\varsigma} + \frac{1}{R_i}A_{i12}w_i + A_{i12}\frac{\partial v_{i0}}{\partial\xi_i} + B_{i12}\frac{\partial\varphi_i}{\partial\xi_i} - N_{i\varsigma}^{\mathrm{PZT}} \end{aligned} \tag{5a}$$

$$\begin{aligned} N_{i\xi} = N_{i22} &= \int_{-\frac{h_i}{2}}^{\frac{h_i}{2}} \sigma_2 \,\mathrm{d}z = \sum_{k=1}^{n}\int_{z_k}^{z_{k+1}} (\overline{Q}_{21}^k\varepsilon_1 + \overline{Q}_{22}^k\varepsilon_2 - \bar{e}_{32}^k E_3^k)\,\mathrm{d}z \\ &= A_{i21}\frac{\partial u_{i0}}{\partial\varsigma} + B_{i21}\frac{\partial\phi_i}{\partial\varsigma} + \frac{1}{R_i}A_{i22}w_i + A_{i22}\frac{\partial v_{i0}}{\partial\xi_i} + B_{i22}\frac{\partial\varphi_i}{\partial\xi_i} - N_{i\xi}^{\mathrm{PZT}} \end{aligned} \tag{5b}$$

$$\begin{aligned} M_{i\varsigma} = M_{i11} &= \int_{-\frac{h_i}{2}}^{\frac{h_i}{2}} \frac{(R_i+z)}{R_i}\sigma_1 z \,\mathrm{d}z = \sum_{k=1}^{n}\int_{z_k}^{z_{k+1}} \frac{(R_i+z)}{R_i}(\overline{Q}_{11}^k\varepsilon_1 + \overline{Q}_{12}^k\varepsilon_2 - \bar{e}_{31}^k E_3^k)z\,\mathrm{d}z \\ &= B_{i11}\frac{\partial u_{i0}}{\partial\varsigma} + D_{i11}\frac{\partial\phi_i}{\partial\varsigma} + \frac{1}{R_i}B_{i12}w_i + B_{i12}\frac{\partial v_{i0}}{\partial\xi_i} + D_{i12}\frac{\partial\varphi_i}{\partial\xi_i} - M_{i\varsigma}^{\mathrm{PZT}} \end{aligned} \tag{5c}$$

$$\begin{aligned} M_{i\xi} = M_{i22} &= \int_{-\frac{h_i}{2}}^{\frac{h_i}{2}} \sigma_2 z \,\mathrm{d}z = \sum_{k=1}^{n}\int_{z_k}^{z_{k+1}} (\overline{Q}_{21}^k\varepsilon_1 + \overline{Q}_{22}^k\varepsilon_2 - \bar{e}_{32}^k E_3^k)z\,\mathrm{d}z \\ &= B_{i21}\frac{\partial u_{i0}}{\partial\varsigma} + D_{i21}\frac{\partial\phi_i}{\partial\varsigma} + \frac{1}{R_i}B_{i22}w_i + B_{i22}\frac{\partial v_{i0}}{\partial\xi_i} + D_{i22}\frac{\partial\varphi_i}{\partial\xi_i} - M_{i\xi}^{\mathrm{PZT}} \end{aligned} \tag{5d}$$

$$\begin{aligned} M_{i\varsigma\xi} = M_{i12} &= \int_{-\frac{h_i}{2}}^{\frac{h_i}{2}} \frac{(R_i+z)}{R_i}\sigma_6 z \,\mathrm{d}z = \sum_{k=1}^{n}\int_{z_k}^{z_{k+1}} \frac{(R_i+z)}{R_i}\overline{Q}_{66}^k\varepsilon_6 z\,\mathrm{d}z \\ &= B_{i661}\frac{\partial u_{i0}}{\partial\xi_i} + D_{i661}\frac{\partial\phi_i}{\partial\xi_i} + \left(B_{i661} + \frac{1}{R_i}D_{i661}\right)\frac{\partial v_{i0}}{\partial\varsigma} + \left(D_{i661} + \frac{1}{R_i}E_{i661}\right)\frac{\partial\varphi_i}{\partial\varsigma} \end{aligned} \tag{5e}$$

$$\begin{aligned} M_{i\xi\varsigma} = M_{i21} &= \int_{-\frac{h_i}{2}}^{\frac{h_i}{2}} \sigma_6 z \,\mathrm{d}z = \sum_{k=1}^{n}\int_{z_k}^{z_{k+1}} \overline{Q}_{66}^k\varepsilon_6 z\,\mathrm{d}z \\ &= B_{i662}\frac{\partial u_{i0}}{\partial\xi_i} + D_{i662}\frac{\partial\phi_i}{\partial\xi_i} + B_{i661}\frac{\partial v_{i0}}{\partial\varsigma} + D_{i661}\frac{\partial\varphi_i}{\partial\varsigma} \end{aligned} \tag{5f}$$

$$\begin{aligned} Q_{i\varsigma\xi} = Q_{i12} &= \int_{-\frac{h_i}{2}}^{\frac{h_i}{2}} \frac{R_i+z}{R_i}\sigma_6 \,\mathrm{d}z = \sum_{k=1}^{n}\int_{z_k}^{z_{k+1}} \frac{R_i+z}{R_i}\overline{Q}_{66}^k\varepsilon_6 \,\mathrm{d}z \\ &= A_{i661}\frac{\partial u_{i0}}{\partial\xi_i} + B_{i661}\frac{\partial\phi_i}{\partial\xi_i} + \left(A_{i661} + \frac{1}{R_i}B_{i661}\right)\frac{\partial v_{i0}}{\partial\varsigma} + \left(B_{i661} + \frac{1}{R_i}D_{i661}\right)\frac{\partial\varphi_i}{\partial\varsigma} \end{aligned} \tag{5g}$$

$$Q_{i\xi_\varsigma} = Q_{i21} = \int_{-\frac{h_i}{2}}^{\frac{h_i}{2}} \sigma_6 \,\mathrm{d}z = \sum_{k=1}^{n} \int_{z_k}^{z_{k+1}} \overline{Q}_{66}^k \varepsilon_6 \,\mathrm{d}z = A_{i662}\frac{\partial u_{i0}}{\partial \xi_i} + B_{i662}\frac{\partial \phi_i}{\partial \xi_i} + A_{i661}\frac{\partial v_{i0}}{\partial \varsigma} + B_{i661}\frac{\partial \varphi_i}{\partial \varsigma} \tag{5h}$$

$$\begin{aligned} Q_{i\xi z} = Q_{iz\xi} = Q_{i23} = Q_{i32} &= \int_{-\frac{h_i}{2}}^{\frac{h_i}{2}} \frac{(R_i+z)}{R_i}\sigma_4 \,\mathrm{d}z = \sum_{k=1}^{n} \int_{z_k}^{z_{k+1}} \frac{(R_i+z)}{R_i} K\overline{Q}_{44}^k \varepsilon_4 \,\mathrm{d}z \\ &= A_{i44}\frac{\partial w_i}{\partial \xi_i} - \frac{1}{R_i}A_{i44}v_{i0} + A_{i44}\varphi_i \end{aligned} \tag{5i}$$

$$Q_{iz_\varsigma} = Q_{i\varsigma z} = Q_{i31} = Q_{i13} = \int_{-\frac{h_i}{2}}^{\frac{h_i}{2}} \sigma_5 \,\mathrm{d}z = \sum_{k=1}^{n} \int_{z_k}^{z_{k+1}} K\overline{Q}_{55}^k \varepsilon_5 \,\mathrm{d}z = A_{i55}\phi_i + A_{i55}\frac{\partial w_{i0}}{\partial \varsigma} \tag{5j}$$

where these resultant forces and moments are general expressions for any parts of pipe joint system. For instance, the above resultant forces and moments will represent the resultant forces and moments of the pipe if the radius $R$ in the general expressions is replaced by $R_p$. In the same manner, the resultant forces and moments for other parts can be obtained. The extensive shell stiffnesses are re-defined and used in the above derivation, i.e. $A_{imn}$, $B_{imn}$ etc. And, the additional resultant forces $N_{ij}^{\mathrm{PZT}}$ and moments $M_{ij}^{\mathrm{PZT}}$ $(i,j=1,2)$ caused by external electric fields that are applied to the integrated piezoelectric layers are defined as

$$N_{c\varsigma}^{\mathrm{PZT}} = N_{c11}^{\mathrm{PZT}} = \sum_{k=1}^{n} \int_{z_k}^{z_{k+1}} \frac{(R_c+z)}{R_c}\bar{e}_{31}^k E_3^k \,\mathrm{d}z \tag{6a}$$

$$N_{c\xi}^{\mathrm{PZT}} = N_{c22}^{\mathrm{PZT}} = \sum_{k=1}^{n} \int_{z_k}^{z_{k+1}} \bar{e}_{32}^k E_3^k \,\mathrm{d}z \tag{6b}$$

$$M_{c\varsigma}^{\mathrm{PZT}} = M_{c11}^{\mathrm{PZT}} = \sum_{k=1}^{n} \int_{z_k}^{z_{k+1}} \frac{(R_c+z)}{R_c}\bar{e}_{31}^k E_3^k z \,\mathrm{d}z \tag{6c}$$

$$M_{c\xi}^{\mathrm{PZT}} = M_{c22}^{\mathrm{PZT}} = \sum_{k=1}^{n} \int_{z_k}^{z_{k+1}} z\bar{e}_{32}^k E_3^k \,\mathrm{d}z \tag{6d}$$

with the electric field applied to the distribution covered surface electrode represented by the 2-D Heaviside step function as

$$E_3^k(\varsigma,\xi) = E_{30}^k[H(\varsigma-\varsigma_0) - H(\varsigma-\varsigma_1)] \times [H(\xi-\xi_0) - H(\xi-\xi_1)] \tag{7}$$

## 3. Representative volume model and equilibrium equations

For a conventional composite pipe joint, it can be approximated as a symmetric structure, as shown in Fig. 1. Then, only half of the joint needs to be modeled, as shown in Fig. 4. A representative infinitesimal element of the joint section is depicted in Fig. 5. In terms of the static equilibrium conditions for each layer as shown in Fig. 5, the fundamental equilibrium equations for any segment of the whole smart pipe joint system (with a rectangular cross section) can be obtained as follows.

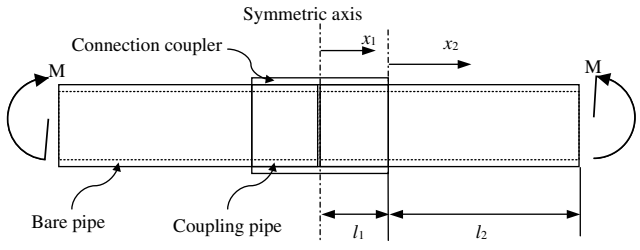


Fig. 4. A schematic view of the different parts of the composite pipe joint system.

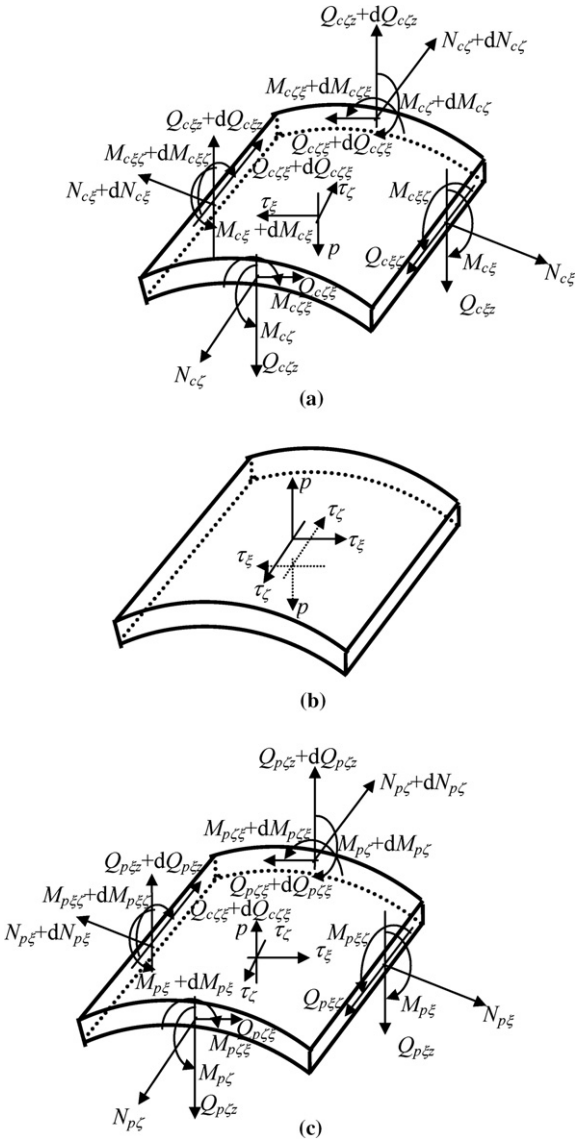


Fig. 5. The stresses and forces on the infinitesimal element of a joint system: (a) the top layer (connection coupler), (b) the adhesive layer, (c) the bottom layer (main pipe).

For the bare part of the main pipe without the adhesive stress distribution effect, the equilibrium equations from the infinitesimal element can be derived, which are in the local coordinate system, as follows:

$$\frac{\partial N_{b\varsigma}}{\partial \varsigma}+\frac{\partial Q_{b\xi\varsigma}}{\partial \xi_p}=0 \tag{8a}$$

$$\frac{\partial N_{b\xi}}{\partial \xi_b}+\frac{Q_{b\xi z}}{R_p}+\frac{\partial Q_{b\xi\varsigma}}{\partial \varsigma}=0 \tag{8b}$$

$$\frac{\partial Q_{b\varsigma z}}{\partial \varsigma}+\frac{\partial Q_{b\xi z}}{\partial \xi_p}-\frac{N_{b\xi}}{R_p}=0 \tag{8c}$$

$$\frac{\partial M_{b\varsigma}}{\partial \varsigma}-Q_{b\varsigma z}+\frac{\partial M_{b\xi\varsigma}}{\partial \xi_p}=0 \tag{8d}$$

$$\frac{\partial M_{b\xi}}{\partial \xi_p}-Q_{b\xi z}+\frac{\partial M_{b\varsigma\xi}}{\partial \varsigma}=0 \tag{8e}$$

For the pipe part covered by the connection coupler, the following equilibrium equations in the local coordinate system can be obtained by considering the effect of the adhesive layer stresses:

$$\frac{\partial N_{p\varsigma}}{\partial \varsigma}+\frac{\partial Q_{p\xi\varsigma}}{\partial \xi_p}=\frac{R_{po}}{R_p}\tau_\varsigma \tag{9a}$$

$$\frac{\partial N_{p\xi}}{\partial \xi_p}+\frac{Q_{p\xi z}}{R_p}+\frac{\partial Q_{p\xi\varsigma}}{\partial \varsigma}=\frac{R_{po}}{R_p}\tau_\xi \tag{9b}$$

$$\frac{\partial Q_{p\varsigma z}}{\partial \varsigma}+\frac{\partial Q_{p\xi z}}{\partial \xi_p}-\frac{N_{p\xi}}{R_p}=-\frac{R_{po}}{R_p}p \tag{9c}$$

$$\frac{\partial M_{p\varsigma}}{\partial \varsigma}-Q_{p\varsigma z}+\frac{\partial M_{p\xi\varsigma}}{\partial \xi_p}=\frac{h_p}{2}\frac{R_{po}}{R_p}\tau_\varsigma \tag{9d}$$

$$\frac{\partial M_{p\xi}}{\partial \xi_p}-Q_{p\xi z}+\frac{\partial M_{p\varsigma\xi}}{\partial \varsigma}=\frac{h_p}{2}\frac{R_{po}}{R_p}\tau_\xi \tag{9e}$$

And in the connection coupler, the equilibrium equations can be described in the local coordinate system by

$$\frac{\partial N_{c\varsigma}}{\partial \varsigma}+\frac{\partial Q_{c\xi\varsigma}}{\partial \xi_c}=-\frac{R_{ci}}{R_c}\tau_\varsigma \tag{10a}$$

$$\frac{\partial N_{c\xi}}{\partial \xi_c}+\frac{Q_{c\xi z}}{R_c}+\frac{\partial Q_{c\xi\varsigma}}{\partial \varsigma}=-\frac{R_{ci}}{R_c}\tau_\xi \tag{10b}$$

$$\frac{\partial Q_{c\varsigma z}}{\partial \varsigma}+\frac{\partial Q_{c\xi z}}{\partial \xi_c}-\frac{N_{c\xi}}{R_c}=\frac{R_{ci}}{R_c}p \tag{10c}$$

$$\frac{\partial M_{c\varsigma}}{\partial \varsigma}-Q_{c\varsigma z}+\frac{\partial M_{c\xi\varsigma}}{\partial \xi_c}=\frac{h_c}{2}\frac{R_{ci}}{R_c}\tau_\varsigma \tag{10d}$$

$$\frac{\partial M_{c\xi}}{\partial \xi_c}-Q_{c\xi z}+\frac{\partial M_{c\varsigma\xi}}{\partial \varsigma}=\frac{h_c}{2}\frac{R_{ci}}{R_c}\tau_\xi \tag{10e}$$

where $R_a$ is the radius of the adhesive layer and $R_a=\frac{R_{ci}+R_{po}}{2}$. $R_{ci}$ and $R_{po}$ are the inner radius of the connection coupler and the outer radius of the main pipe, i.e. the top and bottom surfaces of the adhesive layer, respectively. Here, $\tau_\zeta$, $\tau_\xi$ and $p$ denote the shear and normal stresses in the adhesive layer in the $\zeta$-axis, $\xi$-axis and $z$-axis, respectively. Evidently, the shear and normal stresses in the adhesive layer are caused by the discontinuity of the relative displacements on the top and bottom surfaces of the adhesive layer. Assuming that the adhesive shear stresses are uniform throughout the thickness of the adhesive layer, the shear stresses $\tau_\zeta$ and $\tau_\xi$ can be obtained from the above assumed displacement fields of the pipe and coupler by using the average values of $\frac{\partial w_c}{\partial \varsigma}$, $\frac{\partial w_p}{\partial \varsigma}$, $\frac{\partial w_c}{\partial \xi_c}$ and $\frac{\partial w_p}{\partial \xi_p}$ in the following forms (Yang et al., 2002):

$$\tau_\varsigma=G_a\left(\frac{u_p-u_c}{h_a}\right)-\frac{G_a}{2}\left(\frac{\partial w_c}{\partial \varsigma}+\frac{\partial w_p}{\partial \varsigma}\right) \tag{11a}$$

$$\tau_\xi=G_a\left(\frac{v_p-v_c}{h_a}\right)-\frac{G_a}{2}\left(\frac{\partial w_p}{\partial \xi_p}+\frac{\partial w_c}{\partial \xi_c}\right)+\frac{G_a}{2}\left(\frac{v_p+v_c}{R_a}\right) \tag{11b}$$

In the same manner, the normal stress $p$ of the adhesive layer can be determined from the relative radial displacements of the pipe and coupler:

$$\begin{aligned}p&=\frac{E_a}{(1+\upsilon_a)(1-2\upsilon_a)}\left[(1-\upsilon_a)\left(\frac{w_c-w_p}{h_a}\right)+\upsilon_a\left(\frac{\varepsilon_{p\varsigma}+\varepsilon_{c\varsigma}}{2}\right)+\upsilon_a\left(\frac{\varepsilon_{p\xi}+\varepsilon_{c\xi}}{2}\right)\right]\\&=\frac{E_a}{(1+\upsilon_a)(1-2\upsilon_a)}\left\{(1-\upsilon_a)\left(\frac{w_c-w_p}{h_a}\right)+\frac{\upsilon_a}{2}\left(\frac{\partial u_{p0}}{\partial \varsigma}+\frac{h_p}{2}\frac{\partial \phi_p}{\partial \varsigma}+\frac{\partial u_{c0}}{\partial \varsigma}-\frac{h_c}{2}\frac{\partial \phi_c}{\partial \varsigma}\right)\right.\\&\left.+\frac{\upsilon_a}{2}\left[\frac{w_p}{R_{po}}+\frac{R_p}{R_{po}}\left(\frac{\partial v_{p0}}{\partial \xi_p}+\frac{h_p}{2}\frac{\partial \varphi_p}{\partial \xi_p}\right)+\frac{w_c}{R_{ci}}+\frac{R_c}{R_{ci}}\left(\frac{\partial v_{c0}}{\partial \xi_c}-\frac{h_c}{2}\frac{\partial \varphi_c}{\partial \xi_c}\right)\right]\right\}\end{aligned} \tag{11c}$$

where $G_a$, $E_a$ and $\upsilon_a$ are the shear modulus, Young's modulus and Poisson's ratio of the adhesive, respectively. $h_a$ is the thickness of the adhesive layer.

Furthermore, considering the symmetric smart pipe joint system under the action of the end force and bending moment, as shown in Fig. 4, the relevant boundary conditions and the continuity conditions can be described for different parts of the joint in details in the following:

At $x_2 = l_2$, when the end of pipe is subjected to an external applied force or a bending moment, the relevant boundary conditions can be represented by

$$N_{b\varsigma} = \widetilde{N}_{b\varsigma}, \quad Q_{b\varsigma\xi} = \widetilde{Q}_{b\varsigma\xi}, \quad Q_{b\varsigma z} = \widetilde{Q}_{b\varsigma z}, \quad M_{b\varsigma} = \widetilde{M}_{b\varsigma}, \quad M_{b\varsigma\xi} = \widetilde{M}_{b\varsigma\xi} \tag{12a}$$

At $x_1 = l_1$, since the end of the coupler is free, the boundary conditions can be expressed as

$$N_{c\varsigma} = 0, \quad Q_{c\varsigma\xi} = 0, \quad Q_{c\varsigma z} = 0, \quad M_{c\varsigma} = 0, \quad M_{c\varsigma\xi} = 0 \tag{12b}$$

At $x_1 = 0$, due to the free end and the symmetry, the boundary conditions for the pipe and coupler can be expressed as

$$N_{p\varsigma} = 0, \quad Q_{p\varsigma\xi} = 0, \quad Q_{p\varsigma z} = 0, \quad M_{p\varsigma} = 0, \quad M_{p\varsigma\xi} = 0 \tag{12c}$$

$$u_{0c\varsigma} = 0, \quad \phi_{c\varsigma} = 0, \quad \frac{\partial v_{0c\varsigma}}{\partial\varsigma} = 0, \quad \frac{\partial\varphi_{c\varsigma}}{\partial\varsigma} = 0, \quad \frac{\partial w_{c\varsigma}}{\partial\varsigma} = 0 \tag{12d}$$

Similarly, at the end of the coupling part of the pipe, i.e. $x_1 = l_1$ and $x_2 = 0$, the continuity conditions between the coupling part and bare part of the pipe can be represented by

$$N_{p\varsigma} = N_{b\varsigma}, \quad Q_{p\varsigma\xi} = Q_{b\varsigma\xi}, \quad Q_{p\varsigma z} = Q_{b\varsigma z}, \quad M_{p\varsigma} = M_{b\varsigma}, \quad M_{p\varsigma\xi} = M_{b\varsigma\xi}, \tag{12e}$$

$$u_{0p\varsigma} = u_{0b\varsigma}, \quad \phi_{p\varsigma} = \phi_{b\varsigma}, \quad \frac{\partial v_{0p\varsigma}}{\partial\varsigma} = \frac{\partial v_{0b\varsigma}}{\partial\varsigma}, \quad \frac{\partial\varphi_{p\varsigma}}{\partial\varsigma} = \frac{\partial\varphi_{b\varsigma}}{\partial\varsigma}, \quad \frac{\partial w_{p\varsigma}}{\partial\varsigma} = \frac{\partial w_{b\varsigma}}{\partial\varsigma} \tag{12f}$$

where the upper "$\sim$" of the above variables denotes the prescribed external forces and moments.

In order to obtain the displacement-based governing equations for the different parts of the composite pipe joint system, the resultant forces and moments (Eq. (5)) and the strain–displacement relationships are substituted into the above equilibrium equations and further the relevant displacement-based governing equations for the different parts of the joint are derived. For example, in the coupled pipe part, the displacement-based governing equations can be expressed in the local coordinate system as

$$\begin{aligned}
&A_{p11}\frac{\partial^2 u_{p0}}{\partial\varsigma^2} + B_{p11}\frac{\partial^2\phi_p}{\partial\varsigma^2} + \frac{1}{R_p}A_{p12}\frac{\partial w_p}{\partial\varsigma} + (A_{p12}+A_{p661})\frac{\partial^2 v_{p0}}{\partial\xi_p\partial\varsigma} + (B_{p12}+B_{p661})\frac{\partial^2\varphi_p}{\partial\xi_p\partial\varsigma}\\
&\quad + A_{p662}\frac{\partial^2 u_{p0}}{\partial\xi_p^2} + B_{p662}\frac{\partial^2\phi_p}{\partial\xi_p^2} = \frac{R_{po}}{R_p}\left[G_a\left(\frac{u_p-u_c}{h_a}\right) - \frac{G_a}{2}\left(\frac{\partial w_c}{\partial\varsigma}+\frac{\partial w_p}{\partial\varsigma}\right)\right]
\end{aligned} \tag{13a}$$

$$\begin{aligned}
&(A_{p21}+A_{p662})\frac{\partial^2 u_{p0}}{\partial\varsigma\partial\xi_p} + (B_{p21}+B_{p662})\frac{\partial^2\phi_p}{\partial\varsigma\partial\xi_p} + \frac{1}{R_p}(A_{p22}+A_{p44})\frac{\partial w_p}{\partial\xi_p}\\
&\quad + A_{p22}\frac{\partial^2 v_{p0}}{\partial\xi_p^2} + B_{p22}\frac{\partial^2\varphi_p}{\partial\xi_p^2} + \frac{1}{R_p}\left(-\frac{1}{R_p}A_{p44}v_{p0} + A_{p44}\varphi_p\right) + A_{p661}\frac{\partial^2 v_{p0}}{\partial\varsigma^2} + B_{p661}\frac{\partial^2\varphi_p}{\partial\varsigma^2}\\
&\quad = \frac{R_{po}}{R_p}\left[G_a\left(\frac{v_p-v_c}{h_a}\right) - \frac{G_a}{2}\left(\frac{\partial w_p}{\partial\xi_p}+\frac{\partial w_c}{\partial\xi_c}\right) + \frac{G_a}{2}\left(\frac{v_p+v_c}{R_a}\right)\right]
\end{aligned} \tag{13b}$$

$$\begin{aligned}
&\left(A_{p55} - \frac{1}{R_p}B_{p21}\right)\frac{\partial\phi_p}{\partial\varsigma} + A_{p55}\frac{\partial^2 w_p}{\partial\varsigma^2} + A_{p44}\frac{\partial^2 w_p}{\partial\xi_p^2} - \frac{1}{R_p}(A_{p44}+A_{p22})\frac{\partial v_{p0}}{\partial\xi_p}\\
&\quad + \left(A_{p44} - \frac{1}{R_p}B_{p22}\right)\frac{\partial\varphi_p}{\partial\xi_p} - \frac{1}{R_p}\left(A_{p21}\frac{\partial u_{p0}}{\partial\varsigma} + \frac{1}{R_p}A_{p22}w_p\right)\\
&\quad = -\frac{R_{po}}{R_p}\frac{E_a}{(1+\upsilon_a)(1-2\upsilon_a)}\left\{(1-\upsilon_a)\frac{w_c-w_p}{h_a} + \frac{\upsilon_a}{2}\left(\frac{\partial u_{p0}}{\partial\varsigma} + \frac{h_p}{2}\frac{\partial\phi_p}{\partial\varsigma} + \frac{\partial u_{c0}}{\partial\varsigma} - \frac{h_c}{2}\frac{\partial\phi_c}{\partial\varsigma}\right)\right.\\
&\qquad \left. + \frac{\upsilon_a}{2}\left[\frac{w_p}{R_{po}} + \frac{R_p}{R_{po}}\left(\frac{\partial v_{p0}}{\partial\xi_p} + \frac{h_p}{2}\frac{\partial\varphi_p}{\partial\xi_p}\right) + \frac{w_c}{R_{ci}} + \frac{R_c}{R_{ci}}\left(\frac{\partial v_{c0}}{\partial\xi_c} - \frac{h_c}{2}\frac{\partial\varphi_c}{\partial\xi_c}\right)\right]\right\}
\end{aligned} \tag{13c}$$

$$B_{p11}\frac{\partial^2 u_{p0}}{\partial\varsigma^2}+D_{p11}\frac{\partial^2\phi_p}{\partial\varsigma^2}+\left(\frac{1}{R_p}B_{p12}-A_{p55}\right)\frac{\partial w_p}{\partial\varsigma}+(B_{p12}+B_{p661})\frac{\partial^2 v_{p0}}{\partial\xi_p\partial\varsigma}$$
$$+(D_{p12}+D_{p661})\frac{\partial^2\varphi_p}{\partial\xi_p\partial\varsigma}-A_{p55}\phi_p+B_{p662}\frac{\partial^2 u_{p0}}{\partial\xi_p^2}+D_{p662}\frac{\partial^2\phi_p}{\partial\xi_p^2}$$
$$=\frac{h_p}{2}\frac{R_{po}}{R_p}\left[G_a\left(\frac{u_p-u_c}{h_a}\right)-\frac{G_a}{2}\left(\frac{\partial w_c}{\partial\varsigma}+\frac{\partial w_p}{\partial\varsigma}\right)\right] \tag{13d}$$

$$(B_{p21}+B_{p661})\frac{\partial^2 u_{p0}}{\partial\varsigma\partial\xi_p}+(D_{p21}+D_{p661})\frac{\partial^2\phi_p}{\partial\varsigma\partial\xi_p}+\left(\frac{1}{R_p}B_{p22}-A_{p44}\right)\frac{\partial w_p}{\partial\xi_p}+B_{p22}\frac{\partial^2 v_{p0}}{\partial\xi_p^2}$$
$$+D_{p22}\frac{\partial^2\varphi_p}{\partial\xi_p^2}-\left(-\frac{1}{R_p}A_{p44}v_{p0}+A_{p44}\varphi_p\right)+\left(B_{p661}+\frac{1}{R_p}D_{p661}\right)\frac{\partial^2 v_{p0}}{\partial\varsigma^2}+\left(D_{p661}+\frac{1}{R_p}E_{p661}\right)\frac{\partial^2\varphi_p}{\partial\varsigma^2}$$
$$=\frac{h_p}{2}\frac{R_{po}}{R_p}\left[G_a\left(\frac{v_p-v_c}{h_a}\right)-\frac{G_a}{2}\left(\frac{\partial w_p}{\partial\xi_p}+\frac{\partial w_c}{\partial\xi_c}\right)+\frac{G_a}{2}\left(\frac{v_p+v_c}{R_a}\right)\right] \tag{13e}$$

Similarly, the displacement-based governing equations for the bare pipe part and connection coupler part can be also obtained in the respective local coordinate systems.

Evidently, based on the above analyses, there are a total 15 second-order differential equations with 30 boundary conditions as shown in Eq. (12), which will be used to determine 15 unknown functions, i.e. $u_{p0}$, $\phi_p$, $v_{p0}$, $\varphi_p$ and $w_p$ in the coupled pipe part, $u_{b0}$, $\phi_b$, $v_{b0}$, $\varphi_b$ and $w_b$ in the bare pipe part, $u_{c0}$, $\phi_c$, $v_{c0}$, $\varphi_c$ and $w_c$ in the connection coupler part. Thus, the problem is closed. In order to obtain the analytical solutions for these differential equations, a coordinate transform is introduced to transform the above differential equations into a uniform coordinate system as follows:

$$\frac{\xi_a}{\xi_p}=\frac{R_a}{R_p}\quad\text{and}\quad\frac{\xi_a}{\xi_c}=\frac{R_a}{R_c} \tag{14}$$

Further some coordinate transform relationships can be represented by

$$\frac{\partial(\bullet)}{\partial\xi_p}=\frac{R_a}{R_p}\frac{\partial(\bullet)}{\partial\xi_a}, \tag{15a}$$
$$\frac{\partial^2(\bullet)}{\partial\xi_p^2}=\left(\frac{R_a}{R_p}\right)^2\frac{\partial^2(\bullet)}{\partial\xi_a^2}; \tag{15b}$$
$$\frac{\partial(\bullet)}{\partial\xi_c}=\frac{R_a}{R_c}\frac{\partial(\bullet)}{\partial\xi_a}, \tag{15c}$$
$$\frac{\partial^2(\bullet)}{\partial\xi_c^2}=\left(\frac{R_a}{R_c}\right)^2\frac{\partial^2(\bullet)}{\partial\xi_a^2}. \tag{15d}$$

where the notation '•' inside the bracket denotes the differential variables.

After applying the above coordinate transforms to the displacement-based governing equations for the three parts in their respective local coordinate system, a new set of governing equations with 15 unknown variables and 30 boundary and continuity conditions are obtained in the uniform coordinate system.

## 4. Analytical solution procedure

Considering the symmetry, anti-symmetry and continuity of the circular geometry and applied loading, the general solutions by the Fourier series in the $\xi_a$-axis can be expressed in the following forms:

$$u_0(\varsigma,\xi)=\sum_n U(\varsigma)\cos\left(\frac{n\xi_a}{R_a}\right) \tag{16a}$$
$$\phi(\varsigma,\xi)=\sum_n \Phi(\varsigma)\cos\left(\frac{n\xi_a}{R_a}\right) \tag{16b}$$

$$v_0(\varsigma,\xi)=\sum_n V(\varsigma)\sin\left(\frac{n\xi_a}{R_a}\right) \tag{16c}$$

$$\varphi(\varsigma,\xi)=\sum_n \Psi(\varsigma)\sin\left(\frac{n\xi_a}{R_a}\right) \tag{16d}$$

$$w(\varsigma,\xi)=\sum_n W(\varsigma)\cos\left(\frac{n\xi_a}{R_a}\right) \tag{16e}$$

It is noted that the above basic solutions are general solutions and suitable for the three different parts of the joint. So far, 15 new unknown variables, $U_p(\varsigma)$, $\Phi_p(\varsigma)$, $V_p(\varsigma)$, $\Psi_p(\varsigma)$, $W_p(\varsigma)$, $U_b(\varsigma)$, $\Phi_b(\varsigma)$, $V_b(\varsigma)$, $\Psi_b(\varsigma)$, $W_b(\varsigma)$, $U_p(\varsigma)$, $\Phi_c(\varsigma)$, $V_c(\varsigma)$, $\Psi_c(\varsigma)$ and $W_c(\varsigma)$, have been introduced. In order to simplify the solution process, it is assumed that the applied bending moment $M$ at the joint end is produced by the normal stress resultant with a cosine distribution around the pipe wall, i.e.

$$\widetilde{N}(\varsigma,\xi)=\widetilde{N}_0(\varsigma)\cos\left(\frac{\xi_a}{R_a}\right)$$

Therefore, the assumed Fourier series solution can be further simplified to contain only one sine or cosine term for the basic solutions. Further, the boundary conditions (Eq. (12a)) can be represented by

$$N_{b\varsigma}=-\frac{\widetilde{M}}{\pi R_b^2}\cos\left(\frac{\xi_a}{R_a}\right),\quad Q_{b\varsigma\xi}=0,\quad Q_{bz\varsigma}=0,\quad M_{b\varsigma}=0,\quad M_{b\varsigma\xi}=0 \tag{12a}$$

After substitution of the above relevant solutions into the governing equations in the uniform coordinate system, the coefficients of sine and cosine are collected to obtain a new set of 15 ordinary differential equations involving the above 15 new variables. Here, the detailed new ordinary differential equations for the coupled pipe part are obtained after collecting the coefficients of sine and cosine in the resultant force equations (13a)–(13e)) in the following forms:

$$\begin{aligned}
&A_{p11}\frac{\partial^2 U_{p0}}{\partial\varsigma^2}+B_{p11}\frac{\partial^2\Phi_p}{\partial\varsigma^2}+\frac{1}{R_p}A_{p12}\frac{\partial W_p}{\partial\varsigma}+(A_{p12}+A_{p661})\frac{n}{R_p}\frac{\partial V_{p0}}{\partial\varsigma}+(B_{p12}+B_{p661})\frac{n}{R_p}\frac{\partial\Psi_p}{\partial\varsigma}\\
&\quad-A_{p662}\left(\frac{n}{R_p}\right)^2U_p-B_{p662}\left(\frac{n}{R_p}\right)^2\Phi_p\\
&\qquad=\frac{R_{po}}{R_p}\left[G_a\left(\frac{U_p-U_c}{h_a}+\frac{h_p\phi_p+h_c\phi_c}{2h_a}\right)-\frac{G_a}{2}\left(\frac{\partial W_c}{\partial\zeta}+\frac{\partial W_p}{\partial\zeta}\right)\right]
\end{aligned} \tag{17a}$$

$$\begin{aligned}
&-(A_{p21}+A_{p662})\frac{n}{R_p}\frac{\partial U_p}{\partial\varsigma}-(B_{p21}+B_{p662})\frac{n}{R_p}\frac{\partial\Phi_p}{\partial\varsigma}-\frac{1}{R_p}(A_{p22}+A_{p44})\frac{n}{R_p}W_p\\
&\quad-A_{p22}\left(\frac{n}{R_p}\right)^2V_p-B_{p22}\left(\frac{n}{R_p}\right)^2\Psi_p+\frac{1}{R_p}\left(-\frac{1}{R_p}A_{p44}V_p+A_{p44}\Psi_p\right)+A_{p661}\frac{\partial^2V_p}{\partial\varsigma^2}+B_{p661}\frac{\partial^2\Psi_p}{\partial\varsigma^2}\\
&\qquad=\frac{R_{po}}{R_p}\left[G_a\left(\frac{V_p-V_c}{h_a}+\frac{h_p\psi_p+h_c\psi_c}{2h_a}\right)+\frac{G_a}{2}\left(\frac{n}{R_p}W_p+\frac{n}{R_c}W_c\right)+\frac{G_a}{2}\left(\frac{V_p+V_c}{R_a}+\frac{h_p\psi_p-h_c\psi_c}{2R_a}\right)\right]
\end{aligned} \tag{17b}$$

$$\begin{aligned}
&\left(A_{p55}-\frac{1}{R_p}B_{p21}\right)\frac{\partial\Phi_p}{\partial\varsigma}+A_{p55}\frac{\partial^2W_p}{\partial\varsigma^2}-\left[A_{p44}\left(\frac{n}{R_p}\right)^2+\frac{1}{R_p^2}A_{p22}\right]W_p-(A_{p44}+A_{p22})\frac{n}{R_p^2}V_p\\
&\quad+\left(A_{p44}\frac{n}{R_p}-B_{p22}\frac{n}{R_p^2}\right)\Psi_p-\frac{1}{R_p}A_{p21}\frac{\partial U_p}{\partial\varsigma}\\
&\qquad=-\frac{R_{po}}{R_p}\frac{E_a}{(1+\upsilon_a)(1-2\upsilon_a)}\left\{(1-\upsilon_a)\frac{W_c-W_p}{h_a}+\frac{\upsilon_a}{2}\left(\frac{\partial U_{p0}}{\partial\varsigma}+\frac{h_p}{2}\frac{\partial\Phi_p}{\partial\varsigma}+\frac{\partial U_{c0}}{\partial\varsigma}-\frac{h_c}{2}\frac{\partial\Phi_c}{\partial\varsigma}\right)\right.\\
&\qquad\left.+\frac{\upsilon_a}{2}\left[\frac{W_p}{R_{po}}+\frac{R_p}{R_{po}}\left(\frac{n}{R_p}V_p+\frac{h_p}{2}\frac{n}{R_p}\Psi_p\right)+\frac{W_c}{R_{ci}}+\frac{R_c}{R_{ci}}\left(\frac{n}{R_c}V_c-\frac{h_c}{2}\frac{n}{R_c}\Psi_c\right)\right]\right\}
\end{aligned} \tag{17c}$$

$$B_{p11}\frac{\partial^2 U_p}{\partial\varsigma^2}+D_{p11}\frac{\partial^2\Phi_p}{\partial\varsigma^2}+\left(\frac{1}{R_p}B_{p12}-A_{p55}\right)\frac{\partial W_p}{\partial\varsigma}+(B_{p12}+B_{p661})\frac{n}{R_p}\frac{\partial V_p}{\partial\varsigma}+(D_{p12}+D_{p661})\frac{n}{R_p}\frac{\partial\Psi_p}{\partial\varsigma}$$
$$-\left[A_{p55}+D_{p662}\left(\frac{n}{R_p}\right)^2\right]\Phi_p-B_{p662}\left(\frac{n}{R_p}\right)^2U_p$$
$$=\frac{h_p}{2}\frac{R_{po}}{R_p}\left[G_a\left(\frac{U_p-U_c}{h_a}+\frac{h_p\phi_p+h_c\phi_c}{2h_a}\right)-\frac{G_a}{2}\left(\frac{\partial W_c}{\partial\zeta}+\frac{\partial W_p}{\partial\zeta}\right)\right] \tag{17d}$$

$$-(B_{p21}+B_{p661})\frac{n}{R_p}\frac{\partial U_p}{\partial\varsigma}-(D_{p21}+D_{p661})\frac{n}{R_p}\frac{\partial\Phi_p}{\partial\varsigma}-\left(\frac{1}{R_p}B_{p22}-A_{p44}\right)\frac{n}{R_p}W_p-\left[B_{p22}\left(\frac{n}{R_p}\right)^2-\frac{1}{R_p}A_{p44}\right]V_p$$
$$-\left[D_{p22}\left(\frac{n}{R_a}\right)^2+A_{p44}\right]\Psi_p+\left(B_{p661}+\frac{1}{R_p}D_{p661}\right)\frac{\partial^2 V_p}{\partial\varsigma^2}+\left(D_{p661}+\frac{1}{R_p}E_{p661}\right)\frac{\partial^2\Psi_p}{\partial\varsigma^2}$$
$$=\frac{h_p}{2}\frac{R_{po}}{R_p}\left[G_a\left(\frac{V_p-V_c}{h_a}+\frac{h_p\psi_p+h_c\psi_c}{2h_a}\right)+\frac{G_a}{2}\left(\frac{n}{R_p}W_p+\frac{n}{R_c}W_c\right)+\frac{G_a}{2}\left(\frac{V_p+V_c}{R_a}+\frac{h_p\psi_p-h_c\psi_c}{2R_a}\right)\right] \tag{17e}$$

In the same manner, the new ordinary differential equations for the connection coupler part and bare pipe part can be obtained.

In order to solve these 15-ordinary differential equations, the state-space method can be employed to simplify these equations and further obtain a new set of first-order state equations by introducing the following variables:

$$Z_1=U_p,\quad Z_2=Z_1'=\frac{\partial U_p}{\partial\varsigma},\quad Z_3=\Phi_p,\quad Z_4=Z_3'=\frac{\partial\Phi_p}{\partial\varsigma},\quad Z_5=V_p,$$
$$Z_6=Z_5'=\frac{\partial V_p}{\partial\varsigma},\quad Z_7=\Psi_p,\quad Z_8=Z_7'=\frac{\partial\Psi_p}{\partial\varsigma},\quad Z_9=W_p,\quad Z_{10}=Z_9'=\frac{\partial W_p}{\partial\varsigma},\quad Z_{11}=U_c,$$
$$Z_{12}=Z_{11}'=\frac{\partial U_c}{\partial\varsigma},\quad Z_{13}=\Phi_c,\quad Z_{14}=Z_{13}'=\frac{\partial\Phi_c}{\partial\varsigma},\quad Z_{15}=V_c,\quad Z_{16}=Z_{15}'=\frac{\partial V_c}{\partial\varsigma},\quad Z_{17}=\Psi_c,$$
$$Z_{18}=Z_{17}'=\frac{\partial\Psi_c}{\partial\varsigma},\quad Z_{19}=W_c,\quad Z_{20}=Z_{19}'=\frac{\partial W_c}{\partial\varsigma};$$
$$X_1=U_b,\quad X_2=X_1'=\frac{\partial U_b}{\partial\varsigma},\quad X_3=\Phi_b,\quad X_4=X_3'=\frac{\partial\Phi_b}{\partial\varsigma},\quad X_5=V_b,$$
$$X_6=X_5'=\frac{\partial V_b}{\partial\varsigma},\quad X_7=\Psi_b,\quad X_8=X_7'=\frac{\partial\Psi_b}{\partial\varsigma},\quad X_9=W_b,\quad X_{10}=X_9'=\frac{\partial W_b}{\partial\varsigma}$$

Using the above introduced new variables, the relevant differential equations for the connection coupler and coupled pipe in the overlap part can be expressed by a state equation as

$$\{Z\}'=[H]\{Z\}+[\Lambda] \tag{18a}$$

Similarly, a state equation for the bare pipe part can be obtained

$$\{X\}'=[M]\{X\} \tag{18b}$$

where the non-zero components of the coefficient matrices $[H]$ and $[M]$ are given in detail in Appendix A. The $20\times1$ dimensions matrix $[\Lambda]$ is related to the actuating piezoelectric layer induced forces and moments due to externally applied electric fields and its non-zero components can be represented by

$$\Lambda(12,1)=\frac{D_{c11}(N_{c\varsigma}^{\mathrm{PZT}})'_{\varsigma}-B_{c11}(M_{c\varsigma}^{\mathrm{PZT}})'_{\varsigma}}{A_{c11}D_{c11}-B_{c11}^2},\quad \Lambda(14,1)=\frac{A_{c11}(M_{c\varsigma}^{\mathrm{PZT}})'_{\varsigma}-B_{c11}(N_{c\varsigma}^{\mathrm{PZT}})'_{\varsigma}}{A_{c11}D_{c11}-B_{c11}^2},$$

$$\Lambda(16,1)=\frac{(D_{c661}+E_{c661}/R_c)(N_{c\xi}^{\mathrm{PZT}})'_{\xi}-B_{c661}(M_{c\xi}^{\mathrm{PZT}})'_{\xi}}{A_{c661}(D_{c661}+E_{c661}/R_c)-B_{c661}(B_{c661}+D_{c661}/R_c)},$$

$$\Lambda(18,1)=\frac{A_{c661}(M_{c\xi}^{\mathrm{PZT}})'_{\xi}-(B_{c661}+D_{c661}/R_c)(N_{c\xi}^{\mathrm{PZT}})'_{\xi}}{A_{c661}(D_{c661}+E_{c661}/R_c)-B_{c661}(B_{c661}+D_{c661}/R_c)},\quad \Lambda(20,1)=-\frac{N_{c\xi}^{\mathrm{PZT}}}{A_{c55}R_c}$$

with the following derivation definitions: $(\bullet)'_x=\frac{\partial(\bullet)}{\partial x}$, $\frac{\partial H(x-x_0)}{\partial x}=\delta(x-x_0)$ and $\frac{\partial^2 H(x-x_0)}{\partial x^2}=\delta'(x-x_0)$.

Thus, the shear and peel stresses in the adhesive layer can be re-written by the introduced state variables in the following matrix forms:

$$\tau_{\varsigma}=\left[\frac{G_a}{h_a},0,0,0,0,0,0,0,0,0,-\frac{G_a}{2},-\frac{G_a}{h_a},0,0,0,0,0,0,0,0,-\frac{G_a}{2}\right]\{Z\} \tag{19a}$$

$$\tau_{\xi}=\left[0,0,0,0,\frac{G_a}{h_a}+\frac{G_a}{2R_a},0,0,0,\frac{G_a}{2}\frac{n}{Rp},0,0,0,0,0,0,-\frac{G_a}{h_a}+\frac{G_a}{2R_a},0,0,0,\frac{G_a}{2}\frac{n}{R_c},0\right]\{Z\} \tag{19b}$$

$$p=\frac{E_a}{(1+\upsilon_a)(1-2\upsilon_a)}\left[0,\frac{\upsilon_a}{2},0,\frac{\upsilon_a}{2}\frac{h_p}{2},\frac{\upsilon_a}{2}\frac{n}{R_{po}},0,\frac{\upsilon_a}{2}\frac{n}{R_{po}}\frac{h_p}{2},0,-\frac{1-\upsilon_a}{h_a}+\frac{\upsilon_a}{2R_{po}},0,\right.$$
$$\left.0,\frac{\upsilon_a}{2},0,-\frac{\upsilon_a}{2}\frac{h_c}{2},\frac{\upsilon_a}{2}\frac{n}{R_{ci}},0,-\frac{\upsilon_a}{2}\frac{n}{R_{ci}}\frac{h_c}{2},0,\frac{1-\upsilon_a}{h_a}+\frac{\upsilon_a}{2R_{ci}},0\right]\{Z\} \tag{19c}$$

Now integrating both sides of Eq. (18a) over dummy variable $\vartheta$ from $\zeta_0$ to $\zeta$, the final solution in the following form are derived:

$$Z(\varsigma)=\mathrm{e}^{\varsigma[H]}\{k_1\}+\mathrm{e}^{\varsigma[H]}\int^{\varsigma}\mathrm{e}^{-\vartheta[H]}[\Lambda]\,\mathrm{d}\vartheta \tag{20a}$$

and the general solution for Eq. (18b) is

$$X(\varsigma)=\mathrm{e}^{\varsigma[M]}\{k_2\} \tag{20b}$$

where $\{k_1\}$ is a vector with 20 unknown coefficients determined by the relevant boundary and continuity conditions at $\varsigma=0$, $l_1$, and, $\{k_2\}$ is a vector with 10 unknown coefficients calculated by the boundary and continuity conditions at $\varsigma=0$, $l_2$, as shown in Eq. (12). With the help of the strain–stress and strain–displacement relationships (Eqs. (2)–(5)), the unknown coefficients $\{k_i\}$ $(i=1,2)$ are determined by the boundary and continuity conditions via the programmed Mathematica software. The peel and shear stress distribution in the adhesive layer of the smart composite pipe joint system can be analytically calculated by Eq. (19).

## 5. Numerical example and discussion

In order to validate the effect and efficiency of the integrated piezoelectric layer on the connection coupler, some detailed numerical analyses have been conducted to confirm the integrity of the smart composite pipe joint system subjected to the bending moment at the end of the joint. The 54-dregree filament-wound E-glass/Derakane 470 composite pipe has been taken as the calculation samples for the pipe and the connection coupler. The material properties and geometric parameters of the composite pipe and coupler, adhesive and piezoelectric ceramics used in the detailed simulations have been assumed as follows:

Composite layer: $E_1=25.2$ GPa, $E_2=7.5$ GPa, $G_{12}=2.4$ GPa, $v_{12}=0.32$;
Epoxy adhesive: $E_a=0.96$ GPa, $G_a=0.34$ GPa, $\mu_3=0.412$;
Piezoelectric materials: $E_{\mathrm{PZT}}=8.4\times10^{10}$ N/m$^2$, $\mu_3=0.22$, $d_{31}=d_{32}=-310\times10^{-12}$ m/V;
Geometric parameters: $l_1=0.0254$ m; $l_2=0.0254$ m; $h_a=0.0254$ mm, $h_p=h_c=2.54$ mm, $R_{pi}=50.8$ mm.

Assuming that the smart connection coupler consists of six plys with the following stacking sequence [Comp/PZT1/Comp/Comp/PZT2/Comp] and relevant lamina thickness $\left[\frac{h_c}{6}/\frac{h_c}{6}/\frac{h_c}{6}/\frac{h_c}{6}/\frac{h_c}{6}/\frac{h_c}{6}\right]$, where the layers

PZT1 and PZT2 are subjected to electric fields $E_3^1$ and $E_3^2$, respectively. In order to validate the developed electro-mechanical coupled analytical model, numerical comparisons are firstly presented between the analytical solution and finite element modeling (FEM) results. A complete model of the smart pipe joint was meshed and simulated by ABAQUS eight-node three-dimensional elasticity element (C3D8) and adhesive element (COH3D8).1 It is seen from Figs. 6 and 7 that, with an applied bending moment 113 N m at the end of this smart joint, the analytical results are close to the FEM results. This suggests that the developed analytical model is reliable. The analytical model can be used to conduct parametric analysis. Thereafter, we utilized the verified analytical model to further consider the smart joint response under the action of coupled electric/mechanical loading.

Subjected to the combined electric/mechanical loading, the peel and shear stress distributions are calculated and the results are shown in Figs. 8 and 9 for the shear stress distribution and Fig. 10 for the peel stress distribution along the $\zeta$ axial direction at $\xi_a = 0$, where $E_3^1 = E_3^2$ is used and taken as Study Case 1. All the numerical results in Figs. 8–10 indicate that the peel/shear stress concentrations always present at the edge in the end region of the joint; however, they can be significantly and adaptively changed by the electric fields applied to the integrated piezoelectric layers. Further, in order to evaluate the effect of different electric fields applied to different piezoelectric layers on the shear/peel stress distributions, numerical simulations are conducted and the results of the maximum stress values are presented in Fig. 11 for four study cases. In Case 1, i.e. $E_3^1 = E_3^2$ which can induce $N_i^{\mathrm{PZT}} \neq 0$ and $M_i^{\mathrm{PZT}} \approx 0$; Case 2, i.e. $E_3^2 = -E_3^1$ which can yield $N_i^{\mathrm{PZT}} \approx 0$ and $M_i^{\mathrm{PZT}} \neq 0$; Case 3, i.e. $E_3^1 \neq 0$ and $E_3^2 = 0$ which means $N_i^{\mathrm{PZT}} \neq 0$ and $M_i^{\mathrm{PZT}} \neq 0$; and Case 4, i.e. $E_3^1 = 0$ and

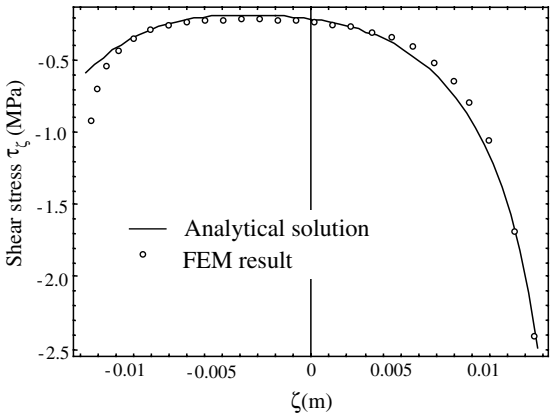


Fig. 6. Numerical comparison of shear stress $\tau_\varsigma$ distribution of a smart joint.

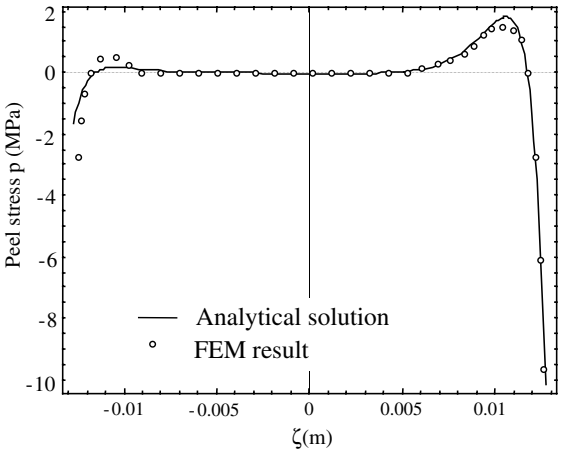


Fig. 7. Numerical comparison of peel stress $p$ distribution of a smart joint.

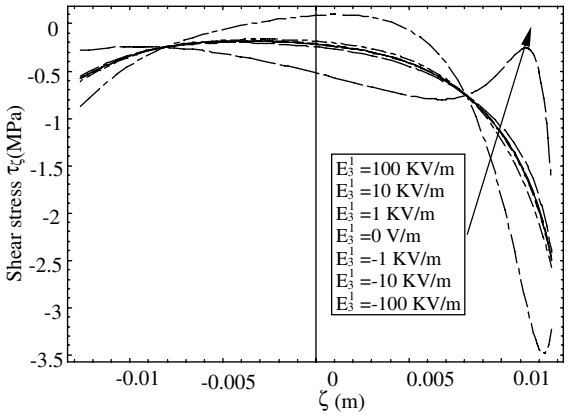


Fig. 8. The influences of the external applied electric fields $E_3^1$ on the shear stress $\tau_\zeta$ distribution along $\zeta$-axis at $\xi$=0 in Case 1.

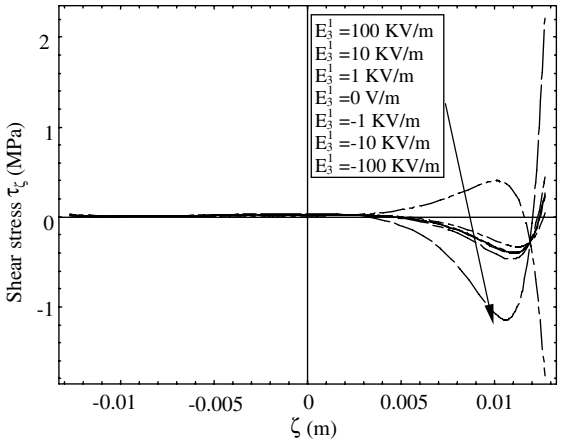


Fig. 9. The influences of the external applied electric fields $E_3^1$ on the shear stress $\tau_\xi$ distribution along $\zeta$-axis at $\xi$=0 in Case 1.

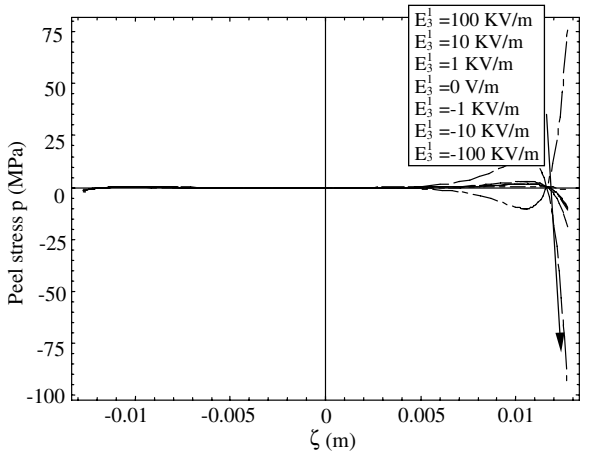


Fig. 10. The effects of the external applied electric fields $E_3^1$ on the peel stress $p$ distribution along $\zeta$-axis at $\xi$=0 in Case 1.

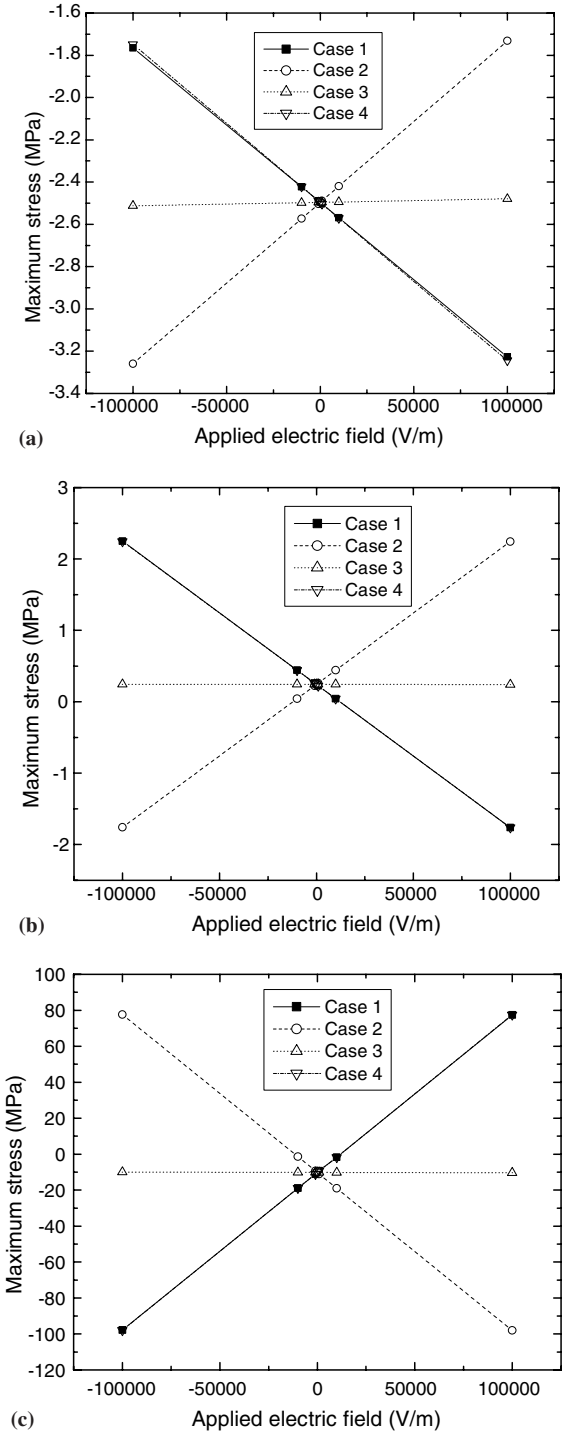


Fig. 11. The comparison of the effect of the applied electric fields $E_3^1$ on the maximum shear stresses $\tau_\zeta$, $\tau_\xi$ (a, b) and maximum peel stress $p$ (c) in Cases 1–4.

$E_3^2 \neq 0$ which indicates $N_i^{\mathrm{PZT}} \neq 0$ and $M_i^{\mathrm{PZT}} \neq 0$. From the numerical results in Fig. 11, it is seen that the applied negative electric fields $E_3^1$ can drastically reduce all the maximum values of shear stresses $\tau_\zeta$, $\tau_\xi$ and peel stress $p$ in Case 1. Specifically, the shear stress $\tau_\zeta$ is reduced from $-3.23$ MPa to $-1.77$ MPa, the shear

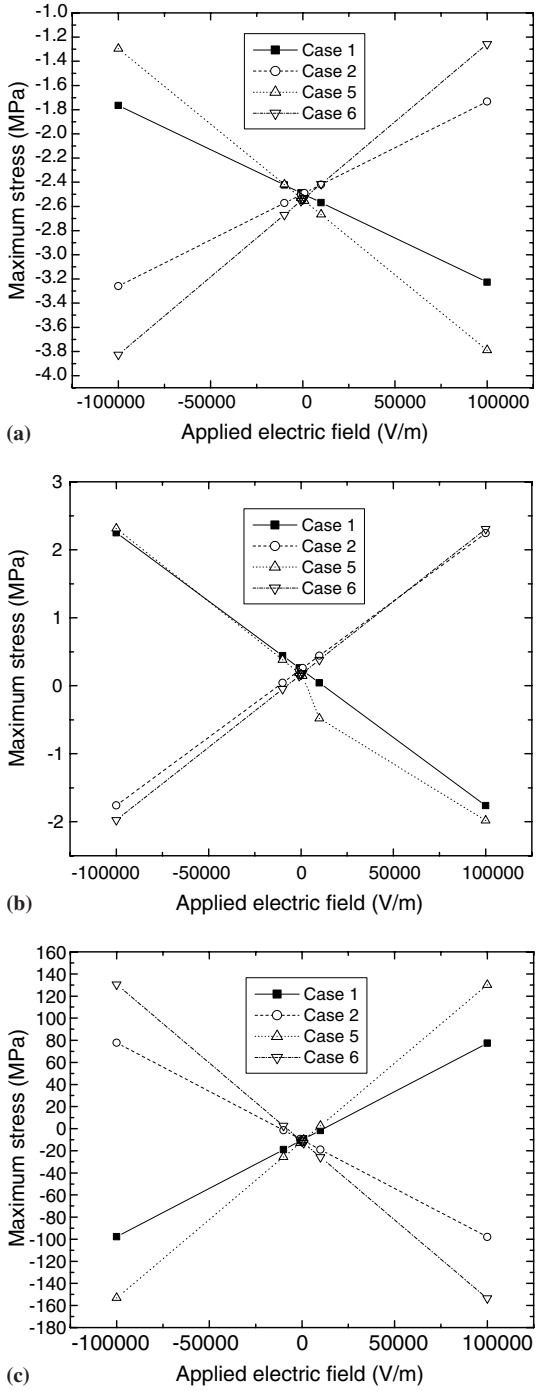


Fig. 12. The influences of the piezoelectric layers' stacking sequence and thickness on the maximum shear stresses $\tau_\xi$, $\tau_\xi$ (a, b) and peel stress $p$ (c) in Cases 1, 2, 5, and 6.

stress $\tau_\xi$ is changed from 2.25 MPa to −1.76 MPa, including zero, and the peel stress is changed from 77.4 MPa (tension) to −97.7 MPa (compression), including zero. This means that the stress concentrations in the adhesive layer can be successfully controlled and even eliminated by applying appropriate electric fields through the integrated piezoelectric layers. To the opposite, a positive electric field $E_3^1$ will increase the maximum values of peel stress $p$ and shear stresses $\tau_\zeta$ and $\tau_\xi$ in Case 1. The same effect is observed in Case 4 as in

Case 1. Compared to Case 1, the applied negative and positive electric fields in Case 2 can induce completely reversed effects, i.e. the applied negative electric fields $E_3^1$ can significantly increase all the maximum values of peel and shear stresses in Case 2 as depicted in Fig. 11. Meanwhile, the applied negative and positive electric fields only have very limited effects on the maximum peel and shear stresses in Case 3. These results indicate that the proposed strength improvement method for the composite pipe joint is designable and can be optimized by controlling the electric fields applied to different piezoelectric layers.

The thickness effect of the integrated piezoelectric layers in the connection coupler is also investigated. Here, it is assumed that the composite connection coupler has the same stacking sequence with different lamina thicknesses $\left[\frac{h_c}{6}/\frac{h_c}{4}/\frac{h_c}{12}/\frac{h_c}{12}/\frac{h_c}{4}/\frac{h_c}{6}\right]$. Similarly, four cases for this geometric parameter are examined, including Case 5, $E_3^1 = E_3^2$, Case 6, $E_3^2 = -E_3^1$, Case 7, $E_3^1 \neq 0$ and $E_3^2 = 0$, and Case 8, $E_3^1 = 0$ and $E_3^2 \neq 0$. Fig. 12 illustrates the detailed numerical results for the thickness effect of the integrated piezoelectric layers on the joint strength enhancement in the composite pipe joint system. From Fig. 12, it is evident that the thicker integrated piezoelectric layers can achieve greater efficiency on changing the maximum peel and shear stresses than the thinner piezoelectric layers. In order to compare and summarize the efficiency of the integrated piezoelectric layers in different study cases, some more detailed comparisons of the maximum peel/shear stresses for all the study cases are presented in Fig. 13–15. From the numerical comparisons, it is again confirmed that the

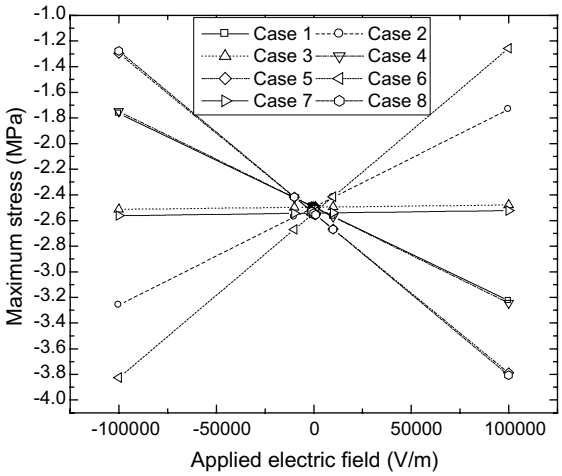


Fig. 13. The detailed efficiency comparisons of the integrated piezoelectric layers on the maximum shear stress $\tau_\zeta$ in all the study cases.

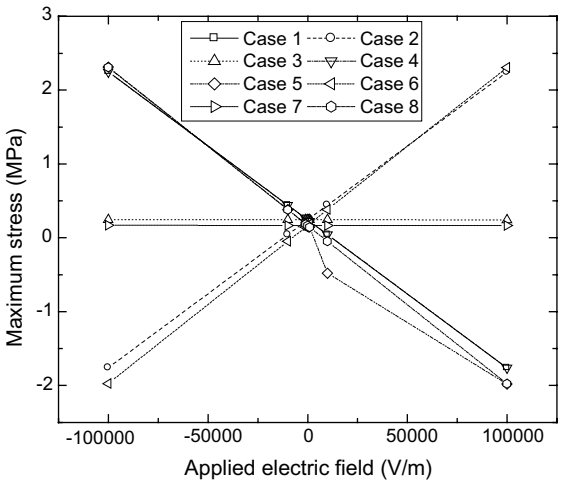


Fig. 14. The detailed efficiency comparisons of the integrated piezoelectric layers on the maximum shear stress $\tau_\xi$ in all the study cases.

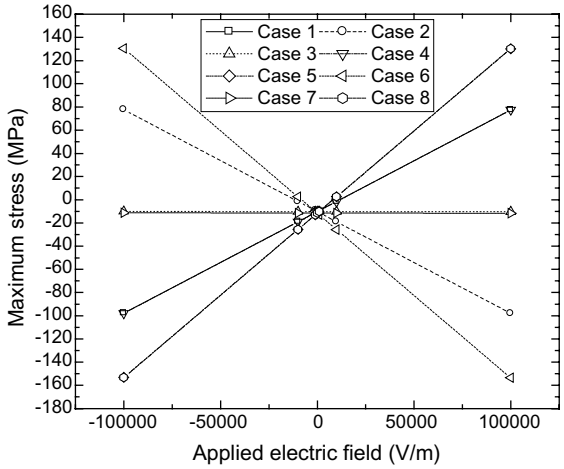


Fig. 15. The detailed efficiency comparisons of the integrated piezoelectric layers on the maximum peel stress $p$ in all the study cases.

thickness of the integrated piezoelectric layers has a significant effect on the maximum peel and shear stresses, and the thicker integrated piezoelectric layers can speed up the enhancement/reduction of the maximum peel/shear stress under the relevant applied electric fields. Due to the overall material properties change of the coupler caused by thickening the integrated piezoelectric layers, the initial maximum peel/shear stresses (i.e. the maximum peel/shear stresses at $E_3^1 = E_3^2 = 0$) have a little increase, as shown in Figs. 13–15. Through the comparisons, it is found that the smart pipe joint structure in Case 6 can achieve a better ability and efficiency in reducing the maximum peel and shears stresses.

From the above detailed numerical analysis, it is evident that the integrated piezoelectric layers can significantly reduce the maximum peel/shear stresses in the adhesive layer with suitable stacking sequence, lamina thickness and applied electric fields. The strength of the smart joint can be adaptively enhanced through a proper design.

## 6. Conclusion

In this paper, design and analysis of an adhesively bonded smart composite pipe joint system was conducted to evaluate the adaptive reduction of the stress concentration in the adhesive layer via the connection coupler integrated with piezoelectric layers as actuators. In order to evaluate the function and efficiency of the integrated piezoelectric layers, an electro-mechanical analytical model was developed to derive fundamental governing equations based on the first-order shear deformation theory. Further, a detailed analytical solution was obtained for the case when the joint was subjected to a bending moment at the end of the joint. The state-space method was employed to obtain the final exact analytical solutions. Both the peel and shear stresses in the adhesive layer were obtained analytically. A finite element analysis was conducted to validate the analytical modeling. Finally, some detailed numerical results were calculated to evaluate the effect of the lamina thickness and applied electric fields on the peel/shear stress concentrations. It is found that, under a proper combination, the peel and shear stress concentrations can be significantly reduced or eliminated in the developed smart composite pipe joint system. It is noted that thermal stress is also a typical loading conditions in practice. This will be a topic in the future studies.

## Appendix A. The element of matrix [$H$] and [$M$]

Based on the introduced new state variables, the resultant governing equations for the overlapping pipe and the connection coupler, as shown in Eqs. (17a)–(17e), are presented in the matrix form as

$$[\Xi]\{Z\}' = [A]\{Z\}, \tag{A.1}$$

further, the matrix $[H]$ in Eq. (18a) is obtained as

$$[H] = [\Xi]^{-1}[A] \tag{A.2}$$

where the non-zero elements of the matrix are as follows:

$$\Xi(i,i) = 1 \quad (i = 1,3,5,\ldots,19);$$

$$\Xi(2,2) = A_{p11}, \quad \Xi(2,4) = B_{p11}, \quad \Xi(4,2) = B_{p11}, \quad \Xi(4,4) = D_{p11}, \quad \Xi(6,6) = A_{p661}, \quad \Xi(6,8) = B_{p661},$$

$$\Xi(8,6) = \left(B_{p661} + \frac{D_{p661}}{R_p}\right), \quad \Xi(8,8) = \left(D_{p661} + \frac{E_{p661}}{R_p}\right), \quad \Xi(10,10) = A_{p55}; \quad \Xi(12,12) = A_{c11},$$

$$\Xi(12,14) = B_{c11}, \quad \Xi(14,12) = B_{c11}, \quad \Xi(14,14) = D_{c11}, \quad \Xi(16,16) = A_{c661}, \quad \Xi(16,18) = B_{c661},$$

$$\Xi(18,16) = \left(B_{c661} + \frac{D_{c661}}{R_c}\right), \quad \Xi(18,18) = \left(D_{c661} + \frac{E_{c661}}{R_c}\right), \quad \Xi(20,20) = A_{c55}$$

and

$$A(i,i+1) = 1 \quad (i = 1,3,5,7,\ldots,19);$$

$$A(2,1) = A_{p662}\left(\frac{n}{R_p}\right)^2 + \underline{\frac{R_{po}}{R_p}\frac{G_a}{h_a}}, \quad A(2,3) = B_{p662}\left(\frac{n}{R_p}\right)^2 + \frac{R_{po}}{R_p}\frac{G_a h_p}{2h_a}, \quad A(2,6) = -(A_{P12} + A_{p661})\frac{n}{R_p},$$

$$A(2,8) = -(B_{P12} + B_{p661})\frac{n}{R_p}, \quad A(2,10) = -\frac{A_{p12}}{R_p} - \underline{\frac{R_{po}}{R_p}\frac{G_a}{2}}, \quad A(2,11) = -\frac{R_{po}}{R_p}\frac{G_a}{h_a}, \quad A(2,13) = \frac{R_{po}}{R_p}\frac{G_a h_c}{2h_a};$$

$$A(2,20) = -\frac{R_{po}}{R_p}\frac{G_a}{2}; \quad A(4,1) = B_{p662}\left(\frac{n}{R_p}\right)^2 + \underline{\frac{h_p}{2}\frac{R_{po}}{R_p}\frac{G_a}{h_a}},$$

$$A(4,3) = A_{p55} + D_{p662}\left(\frac{n}{R_p}\right)^2 + \frac{h_p}{2}\frac{R_{po}}{R_p}\frac{G_a h_p}{2h_a}, \quad A(4,6) = -(B_{P12} + B_{p661})\frac{n}{R_p},$$

$$A(4,8) = -(D_{P12} + D_{p661})\frac{n}{R_p}, \quad A(4,10) = -\left(\frac{B_{p12}}{R_p} - A_{p55}\right) - \underline{\frac{h_a}{2}\frac{R_{po}}{R_p}\frac{G_a}{2}}, \quad A(4,11) = -\frac{h_p}{2}\frac{R_{po}}{R_p}\frac{G_a}{h_a},$$

$$A(4,13) = \frac{h_p}{2}\frac{R_{po}}{R_p}\frac{G_a h_c}{2h_a}, \quad A(4,20) = -\frac{h_p}{2}\frac{R_{po}}{R_p}\frac{G_a}{2}; \quad A(6,2) = (A_{P21} + A_{p662})\frac{n}{R_p}, \quad A(6,4) = (B_{P21} + B_{p662})\frac{n}{R_p},$$

$$A(6,5) = A_{p22}\left(\frac{n}{R_p}\right)^2 + \frac{A_{p44}}{R_p^2} + \underline{\frac{R_{po}}{R_p}\left(\frac{G_a}{h_a} + \frac{G_a}{2R_a}\right)}, \quad A(6,7) = B_{p22}\left(\frac{n}{R_p}\right)^2 - \frac{A_{p44}}{R_p^2} + \frac{R_{po}}{R_p}\left(\frac{G_a h_p}{2h_a} + \frac{G_a h_p}{4R_a}\right),$$

$$A(6,9) = (A_{p22} + A_{p44})\frac{n}{R_p^2} + \underline{\frac{R_{po}}{R_p}\frac{G_a n}{2R_p}}, \quad A(6,15) = \frac{R_{po}}{R_p}\left(-\frac{G_a}{h_a} + \frac{G_a}{2R_a}\right), \quad A(6,17) = \frac{R_{po}}{R_p}\left(\frac{G_a h_c}{2h_a} - \frac{G_a h_c}{4R_a}\right),$$

$$A(6,19) = \frac{R_{po}}{R_p}\frac{G_a n}{2R_c}. \quad A(8,2) = (B_{P21} + B_{p662})\frac{n}{R_p}, \quad A(8,4) = (D_{P21} + D_{p662})\frac{n}{R_p},$$

$$A(8,5) = B_{p22}\left(\frac{n}{R_p}\right)^2 - \frac{A_{p44}}{R_p^2} + \underline{\frac{2R_{po}}{h_p R_p}\left(\frac{G_a}{h_a} + \frac{G_a}{2R_a}\right)}, \quad A(8,7) = D_{p22}\left(\frac{n}{R_p}\right)^2 - A_{p44} + \frac{h_p}{2}\frac{R_{po}}{R_p}\left(\frac{G_a h_p}{2h_a} + \frac{G_a h_p}{4R_a}\right),$$

$$A(8,9) = \left(\frac{B_{p22}}{R_p} - A_{p44}\right)\frac{n}{R_p} + \underline{\frac{h_p}{2}\frac{R_{po}}{R_p}\frac{G_a n}{2R_p}}, \quad A(8,15) = \frac{h_p}{2}\frac{R_{po}}{R_p}\left(-\frac{G_a}{h_a} + \frac{G_a}{2R_a}\right), \quad A(8,17) = \frac{h_p}{2}\frac{R_{po}}{R_p}\left(\frac{G_a h_c}{2h_a} - \frac{G_a h_c}{4R_a}\right);$$

$$A(8,19) = \frac{h_c}{2}\frac{R_{po}}{R_p}\frac{G_a n}{2R_c}, \quad A(10,2) = \frac{A_{p21}}{R_p} + \underline{a\frac{\upsilon_a}{2}}, \quad A(10,4) = -\left(A_{p55} - \frac{B_{p21}}{R_p}\right) + \underline{a\frac{\upsilon_a}{2}\frac{h_p}{2}},$$

$$A(10,5) = (A_{p44} + A_{p22})\frac{n}{R_p^2} + \underline{a\frac{\upsilon_a}{2}\frac{R_{po}}{R_p}\frac{n}{R_p}}, \quad A(10,7) = -\left(A_{p44}\frac{n}{R_p} - B_{p22}\frac{n}{R_p^2}\right) + \underline{a\frac{\upsilon_a}{2}\frac{R_{po}}{R_p}\frac{n}{R_p}\frac{h_p}{2}},$$

$$A(10,9) = A_{p44}\frac{n^2}{R_p^2} + \frac{A_{p22}}{R_p^2} - \underline{a\frac{(1-\upsilon_a)}{h_a} + a\frac{\upsilon_a}{2}\frac{1}{R_{po}}}, \quad A(10,12) = a\frac{\upsilon_a}{2}, \quad A(10,14) = -a\frac{\upsilon_a}{2}\frac{h_c}{2},$$

$$A(10,15)=a\frac{\upsilon_a}{2}\frac{R_{ci}}{R_c}\frac{n}{R_c},\quad A(10,17)=-a\frac{\upsilon_a}{2}\frac{R_{ci}}{R_c}\frac{n}{R_c}\frac{h_c}{2},\quad A(10,19)=a\frac{(1-\upsilon_a)}{h_a}+a\frac{\upsilon_a}{2}\frac{1}{R_{ci}};$$

$$A(12,1)=-\frac{R_{ci}}{R_c}\frac{G_a}{h_a},\quad A(12,3)=-\frac{R_{ci}}{R_c}\frac{G_a h_p}{2h_a};\quad A(12,10)=\frac{R_{ci}}{R_c}\frac{G_a}{2},\quad A(12,11)=A_{c662}\left(\frac{n}{R_c}\right)^2+\frac{R_{ci}}{R_c}\frac{G_a}{h_a},$$

$$A(12,13)=B_{c662}\left(\frac{n}{R_c}\right)^2-\frac{R_{ci}}{R_c}\frac{G_a h_c}{2h_a},\quad A(12,16)=-(A_{c12}+A_{c661})\frac{n}{R_c},\quad A(12,18)=-(B_{c12}+B_{c661})\frac{n}{R_c},$$

$$A(12,20)=-\frac{A_{c12}}{R_c}+\frac{R_{ci}}{R_c}\frac{G_a}{2};\quad A(14,1)=\frac{h_c}{2}\frac{R_{ci}}{R_c}\frac{G_a}{h_a},\quad A(14,3)=\frac{h_c}{2}\frac{R_{ci}}{R_c}\frac{G_a h_p}{2h_a},\quad A(14,10)=-\frac{h_c}{2}\frac{R_{ci}}{R_c}\frac{G_a}{2},$$

$$A(14,11)=B_{c662}\left(\frac{n}{R_c}\right)^2+\frac{h_c}{2}\frac{R_{ci}}{R_c}\frac{G_a}{h_a},\quad A(14,13)=A_{c55}+B_{c662}\left(\frac{n}{R_c}\right)^2+\frac{h_c}{2}\frac{R_{ci}}{R_c}\frac{G_a h_c}{2h_a},$$

$$A(14,16)=-(B_{c12}+B_{c661})\frac{n}{R_c},\quad A(14,18)=-(D_{c12}+D_{c661})\frac{n}{R_c}$$

$$A(14,20)=-\left(\frac{A_{c12}}{R_c}-A_{c55}\right)-\frac{h_c}{2}\frac{R_{ci}}{R_c}\frac{G_a}{2};\quad A(16,5)=\frac{R_{ci}}{R_c}\left(\frac{G_a}{h_a}+\frac{G_a}{2R_a}\right),\quad A(16,7)=-\frac{R_{ci}}{R_c}\left(\frac{G_a h_p}{2h_a}+\frac{G_a h_p}{4R_a}\right);$$

$$A(16,9)=-\frac{R_{ci}}{R_c}\frac{G_a n}{2R_c},\quad A(16,12)=(A_{c21}+A_{c662})\frac{n}{R_c},\quad A(16,14)=(B_{c21}+B_{c662})\frac{n}{R_c},$$

$$A(16,15)=A_{c22}\left(\frac{n}{R_c}\right)^2+\frac{A_{c44}}{R_c^2}+\frac{R_{ci}}{R_c}\left(\frac{G_a}{h_a}-\frac{G_a}{2R_a}\right),\quad A(16,17)=B_{c22}\left(\frac{n}{R_c}\right)^2-\frac{A_{c44}}{R_c^2}-\frac{R_{ci}}{R_c}\left(\frac{G_a h_c}{2h_a}-\frac{G_a h_c}{4R_a}\right),$$

$$A(16,19)=(A_{c22}+A_{c44})\frac{n}{R_c^2}-\frac{R_{ci}}{R_c}\frac{G_a n}{2R_c};\quad A(18,5)=\frac{h_c}{2}\frac{R_{ci}}{R_c}\left(\frac{G_a}{h_a}+\frac{G_a}{2R_a}\right),\quad A(18,7)=\frac{h_c}{2}\frac{R_{ci}}{R_c}\left(\frac{G_a h_p}{2h_a}+\frac{G_a h_p}{4R_a}\right),$$

$$A(18,9)=\frac{h_c}{2}\frac{R_{ci}}{R_c}\frac{G_a n}{2R_c},\quad A(18,12)=(B_{c21}+B_{c662})\frac{n}{R_c},\quad A(18,14)=(D_{c21}+D_{c662})\frac{n}{R_c},$$

$$A(18,15)=B_{c22}\left(\frac{n}{R_c}\right)^2-\frac{A_{c44}}{R_c^2}+\frac{h_c}{2}\frac{R_{ci}}{R_c}\left(-\frac{G_a}{h_a}+\frac{G_a}{2R_a}\right),\quad A(18,17)=D_{c22}\left(\frac{n}{R_c}\right)^2+A_{c44}+\frac{h_c}{2}\frac{R_{ci}}{R_c}\left(\frac{G_a h_c}{2h_a}-\frac{G_a h_c}{4R_a}\right),$$

$$A(18,19)=\left(\frac{B_{c22}}{R_c}-A_{c44}\right)\frac{n}{R_c}+\frac{h_c}{2}\frac{R_{ci}}{R_c}\frac{G_a n}{2R_c};\quad A(20,2)=b\frac{\upsilon_a}{2},\quad A(20,4)=b\frac{\upsilon_a}{2}\frac{h_p}{2},$$

$$A(20,5)=b\frac{\upsilon_a}{2}\frac{R_{po}}{R_p}\frac{n}{R_p},\quad A(20,7)=b\frac{\upsilon_a}{2}\frac{R_{po}}{R_p}\frac{n}{R_p}\frac{h_p}{2},\quad A(20,9)=-b\frac{(1-\upsilon_a)}{h_a}+b\frac{\upsilon_a}{2}\frac{1}{R_{po}},$$

$$A(20,12)=\frac{A_{c21}}{R_c}+b\frac{\upsilon_a}{2},\quad A(20,14)=-\left(A_{c55}-\frac{B_{c21}}{R_c}\right)-b\frac{\upsilon_a}{2}\frac{h_c}{2},$$

$$A(20,15)=(A_{c44}+A_{c22})\frac{n}{R_c^2}+b\frac{\upsilon_a}{2}\frac{R_{ci}}{R_c}\frac{n}{R_c},\quad A(20,17)=-\left(A_{c44}\frac{n}{R_c}-B_{c22}\frac{n}{R_c^2}\right)-b\frac{\upsilon_a}{2}\frac{R_{ci}}{R_c}\frac{n}{R_c}\frac{h_c}{2},$$

$$A(20,19)=A_{c44}\frac{n^2}{R_c^2}+\frac{A_{c22}}{R_c^2}+b\frac{(1-\upsilon_a)}{h_a}+b\frac{\upsilon_a}{2}\frac{1}{R_{ci}}$$

with the following definitions:

$$a=-\frac{R_{po}}{R_p}\frac{E_a}{(1+\upsilon_a)(1-2\upsilon_a)},\quad b=\frac{R_{ci}}{R_c}\frac{E_a}{(1+\upsilon_a)(1-2\upsilon_a)}.$$

Similarly, the displacement based governing equations for the bare pipe part can be obtained by neglecting the right terms of Eqs. (17a)–(17e), and are further represented in the matrix form as follows:

$$[\Pi]\{X\}'=[B]\{X\},\tag{A.3}$$

where the $[\Pi]$ is a $10\times10$ dimensional matrix, in which the elements are equal to the relevant elements of the first 10 columns in the first 10 rows of matrix $[\Xi]$. The matrix $[B]$ is also a $10\times10$ dimensional matrix, which

are equal to the part of the first 10 rows × 10 columns of matrix $[A]$, only by neglecting the underlined terms in the relevant elements. Then, the matrix $[M]$ can be obtained by

$$[M] = [\Pi]^{-1}[B] \tag{A.4}$$

## References


Adams, R.D., Peppiatt, N.A., 1977. Stress analysis of adhesive bonded tubular lap joint. J. Adhesion 9, 1–18.

Adams, R.D., Wake, W.C., 1984. Structural Adhesive Joints in Engineering. Elsevier, London.

Albat, A.M., Romilly, D.P., 1999. A direct linear-elastic analysis of double symmetric bonded joints and reinforcements. Compos. Sci. Technol. 59, 1127–1137.

Batra, R.C., Geng, T.S., 2001. Enhancement of the dynamic buckling load for a plate by using piezoceramic actuators. Smart Mater. Struct. 10, 925–933.

Chen, D., Cheng, S., 1992a. Torsional stress in tubular lap joints. Int. J. Solids Struct. 29 (7), 845–853.

Chen, D., Cheng, S., 1992b. Torsional stresses in tubular lap joints with tapered adherends. J. Eng. Mech. – ASCE 118 (9), 1962–1973.

Cheng, J.Q., Taheri, F., 2005. A novel smart adhesively bonded joint system. Smart Mater. Struct. 14 (5), 971–981.

Cheng, J.Q., Taheri, F., 2006. A smart single-lap adhesive joint integrated with partially distributed piezoelectric patches. Int. J. Solids Struct. 43 (5), 1079–1092.

Cheng, S., Chen, D., Shi, Y.P., 1991. Analysis of adhesive-bonded joints with nonidentical adherends. J. Eng. Mech. 117 (3), 605–623.

Cheng, J.Q., Qian, C.F., Zhao, M.H., et al., 2000. Effects of electric fields on the bending behavior of PZT-5H piezoelectric laminates. Smart Mater. Struct. 9, 824–831.

Cheng, J.Q., Wang, B., Du, S.Y., 2005a. A theoretical analysis of piezoelectric/ composite laminate with larger-amplitude deflection effect, Part I: Fundamental equations. Int. J. Solids Struct. 42 (24–25), 6166–6180.

Cheng, J.Q., Wang, B., Du, S.Y., 2005b. A theoretical analysis of piezoelectric/composite laminate with large-amplitude deflection effect, Part II: Hermite differential quadrature method and application. Int. J. Solids Struct. 42 (24–25), 6181–6201.

Cheng, J.Q., Wu, X.X., Li, G.Q., Taheri, F., Pang, S.S., in press. Design and analysis of a smart adhesive single-strap joint system integrated with the piezoelectric reinforced composite layers. Compos. Sci. Technol.

Choi, J.H., Lee, D.G., 1997. Torque capacity of co-cured tubular lap joints. J. Compos. Mater. 31 (14), 1381–1396.

Crawley, E.F., de Luis, J., 1987. Use of piezoelectric actuators as elements of intelligent structures. AIAA J. 25, 1373–1385.

Goland, M., Reissner, E., 1944. The stress in cemented joints. J. Appl. Mech. 11, A17–A27.

Hart-Smith, L.J., 1973. Adhesive-bonded single lap joints. NASA, CR-112236.

Hart-Smith, L.J., 1983. Designing to minimize peel stresses in adhesive-bonded joints. In: Johnson, W.S. (Ed.), Delamination and Debonding of Materials. ASTM STP 876, 238–266.

Lee, C.K., Moon, F.C., 1990. Modal sensors and actuators. J. Appl. Mech. 57, 434–441.

Lee, D.G., Oh, J.H., 1999. Nonlinear analysis of the torque transmission capability of adhesively bonded tubular lap joints. J. Adhesion 71 (1), 81–106.

Luo, Q.T., Tong, L., 2002. Exact static solutions to piezoelectric smart beams including peel stresses, I: Theoretical formulation. Int. J. Solids Struct. 39, 4677–4695.

Pugno, N., Carpinteri, A., 2003. Tubular adhesive joints under axial load. J. Appl. Mech. – Trans. ASME 70 (6), 832–839.

Roberts, T.M., 1989. Shear and normal stresses in adhesive joints. J. Eng. Mech. 115 (11), 2460–2479.

Tsai, M.Y., Morton, J., 1994. An evaluation of analytical and numerical solutions to the single-lap joint. Int. J. Solids Struct. 31 (18), 2537–2563.

Wu, X.X., Cheng, J.Q., Wang, B., 2001. Influence of applied electric field on the energy release rate for cracked PZT/elastic laminates. Smart Mater. Struct. 10 (5), 970–978.

Yang, C.D., 2000. Design and analysis of composite pipe joints under tensile loading. J. Compos. Mater. 34 (4), 332–349.

Yang, C.D., Huang, H., et al., 2002. Stress model of composite pipe joints under bending. J. Compos. Mater. 36 (11), 1331–1348.

Zhou, Z.G., Wang, B., 2002. The behavior of two parallel symmetry permeable interface cracks in a piezoelectric layer bonded to two half piezoelectric materials planes. Int. J. Solids. Struct. 39 (17), 4485–4500.

Zhou, Z.G., Wang, B., Sun, Y.G., 2003. Investigation of the dynamic behavior of two parallel symmetric cracks in piezoelectric materials use of non-local theory. Int. J. Solids Struct. 40 (3), 747–762.